

Atomistic modeling-based design of novel materials

Holec, David; Zhou, Liangcai; Riedl, Helmut; Koller, Christian M.; Mayrhofer, Paul H.; Friák, Martin; Šob, Mojmír; Körmann, Fritz; Neugebauer, Jörg; Music, Denis

DOI

[10.1002/adem.201600688](https://doi.org/10.1002/adem.201600688)

Publication date

2017

Document Version

Final published version

Published in

Advanced Engineering Materials

Citation (APA)

Holec, D., Zhou, L., Riedl, H., Koller, C. M., Mayrhofer, P. H., Friák, M., Šob, M., Körmann, F., Neugebauer, J., Music, D., Hartmann, M. A., & Fischer, F. D. (2017). Atomistic modeling-based design of novel materials. *Advanced Engineering Materials*, 19(4), Article 1600688. <https://doi.org/10.1002/adem.201600688>

Important note

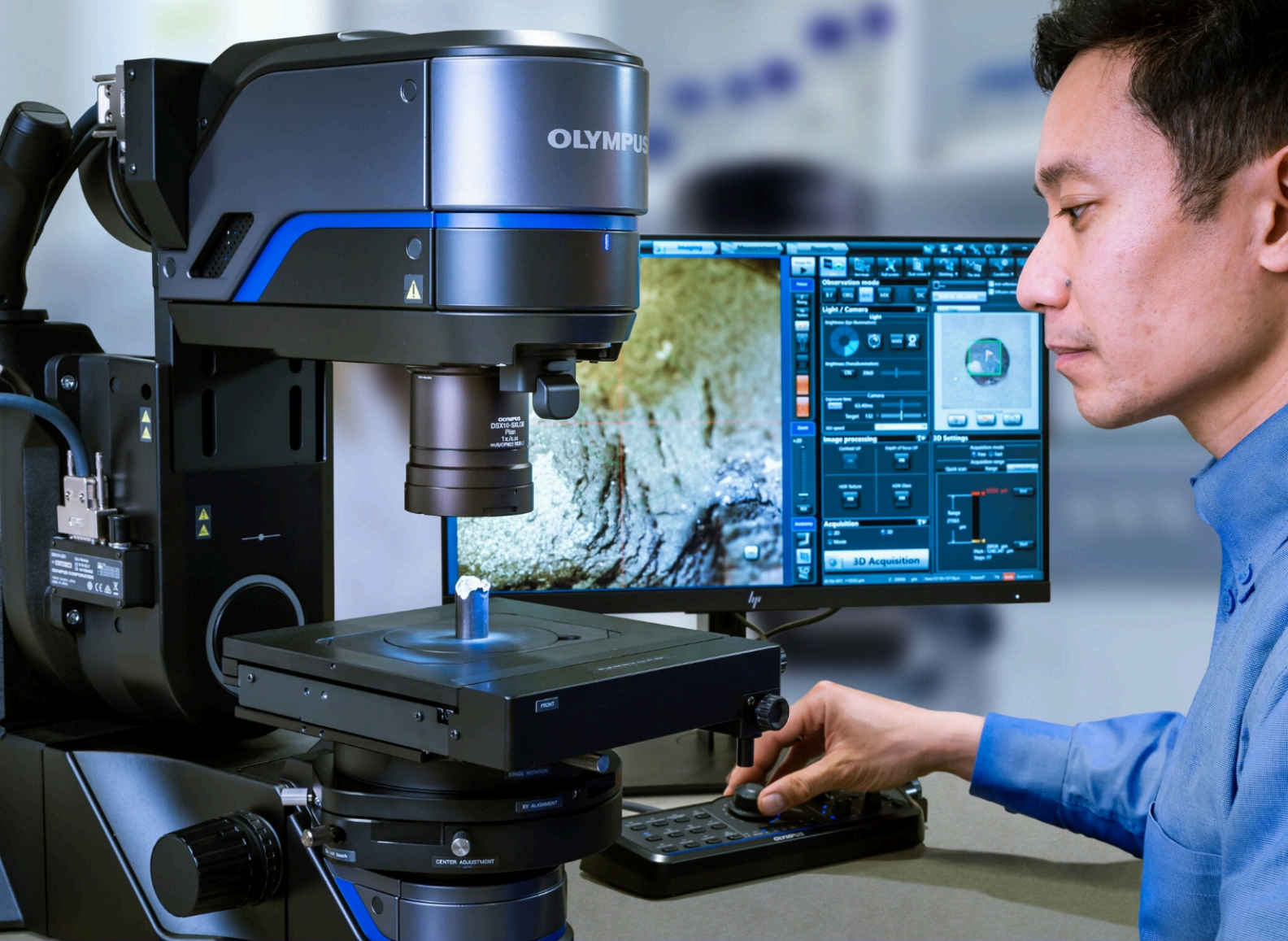
To cite this publication, please use the final published version (if applicable).
Please check the document version above.

Copyright

Other than for strictly personal use, it is not permitted to download, forward or distribute the text or part of it, without the consent of the author(s) and/or copyright holder(s), unless the work is under an open content license such as Creative Commons.

Takedown policy

Please contact us and provide details if you believe this document breaches copyrights.
We will remove access to the work immediately and investigate your claim.



Science Meets Technology with Advanced Optical Metrology

Access in-depth information on methods and applications in the R&D field of optical metrology through free to access article digests of recent peer-reviewed publications and more.

Discover advancedopticalmetrology.com now!

OLYMPUS

WILEY

DOI: 10.1002/adem.201600688

Atomistic Modeling-Based Design of Novel Materials**

By David Holec,* Liangcai Zhou, Helmut Riedl, Christian M. Koller, Paul H. Mayrhofer, Martin Friák, Mojmir Šob, Fritz Körmann, Jörg Neugebauer, Denis Music, Markus A. Hartmann and Franz D. Fischer

Modern materials science increasingly advances via a knowledge-based development rather than a trial-and-error procedure. Gathering large amounts of data and getting deep understanding of non-trivial relationships between synthesis of materials, their structure and properties is experimentally a tedious work. Here, theoretical modeling plays a vital role. In this review paper we briefly introduce modeling approaches employed in materials science, their principles and fields of application. We then focus on atomistic modeling methods, mostly quantum mechanical ones but also Monte Carlo and classical molecular dynamics, to demonstrate their practical use on selected examples.

[*] Dr. D. Holec

Department of Physical Metallurgy and Materials Testing,
Franz-Josef-Straße 18, A-8700 Leoben, Austria

E-mail: david.holec@unileoben.ac.at

Dr. L. Zhou, Dr. H. Riedl, Dr. C. M. Koller, Prof. P. H. Mayrhofer

Institute of Materials Science and Technology, TU Wien,
Getreidemarkt 9, A-1060 Vienna, Austria

Dr. H. Riedl, Dr. C. M. Koller

Christian Doppler Laboratory for Application Oriented Coating
Development, TU Wien, Getreidemarkt 9, A-1060 Vienna,
Austria

Dr. M. Friák, Prof. M. Šob

Institute of Physics of Materials, Academy of Sciences of the
Czech Republic, v.v.i., Žitkova 22, CZ-616 62 Brno, Czech
Republic

Dr. M. Friák, Prof. M. Šob

Central European Institute of Technology, CEITEC MU,
Masaryk University, Kamenice 753/5, CZ-625 00 Brno, Czech
Republic

Prof. M. Šob

Department of Chemistry, Faculty of Science, Masaryk
University, Kotlářská 2, CZ-611 37 Brno, Czech Republic

Dr. F. Körmann, Prof. J. Neugebauer

Max-Planck-Institut für Eisenforschung GmbH, Max-Planck-
Straße 1, D-40237 Düsseldorf, Germany

Dr. F. Körmann

Department of Materials Science and Engineering, Delft
University of Technology, Mekelweg 2, NL-2628 CD Delft,
The Netherlands

Dr. D. Music

Materials Chemistry, RWTH Aachen University, Kopernikus-
straße 10, D-52074 Aachen, Germany

Dr. M. A. Hartmann

Faculty of Physics, University of Vienna, Sensengasse 8/9, A-
1090 Vienna, Austria

Prof. F. D. Fischer

Institute of Mechanics, Franz-Josef-Straße 18, A-8700 Leoben,
Austria

[**] The financial support by the START Program (Y371) of the Austrian Science Fund (FWF) is greatly acknowledged [D.H., L.Z., P.H.M.]. Part of this research was supported by the Academy of Sciences of the Czech Republic through the Fellowship of J. E. Purkyně [M.F.], by the Ministry of Education, Youth, and Sports of the Czech Republic under the Project CEITEC 2020 (LQ1601) [M.F., M.Š.] and further by the Czech Science Foundation, Projects GA 14-22490S, and GA 16-24711S [M.F., M.Š.]. F.K. gratefully acknowledges funding by the scholarship KO 5080/1-1 of the Deutsche Forschungsgemeinschaft (DFG). D.M. acknowledges the Collaborative Research Center SFB-TR 87/2 "Pulsed high power plasmas for the synthesis of nanostructured functional layers" of the DFG. The computational results presented have been achieved in part using the Vienna Scientific Cluster (VSC). Other computational resources were provided by the Ministry of Education, Youth, and Sports of the Czech Republic under the Projects CESNET (Project No. LM2015042), CERIT-Scientific Cloud (Project No. LM2015085), and IT4Innovations National Supercomputer Center (Project No. LM2015070), within the program Projects of Large Research, Development and Innovations Infrastructures.



David Holec got BSc degrees in Mathematics (2002) and Physics (2003) and an MSc degree in Condensed Matter Physics (2005) from Masaryk University in Brno, Czech Republic. After receiving a PhD in Materials Science from the University of Cambridge, UK, he joined Department of Physical Metallurgy and Materials Testing at Montanuniversität Leoben, Austria, in 2008.

He completed his Habilitation in 2016. Since 2012 he is a group leader for Materials Science Modeling. He has (co-) authored over 70 peer-reviewed papers. His main activities include (but are not limited to) Density Functional Theory calculations of structural and functional properties of disordered systems.

1. Introduction

The advancement of computational power in the last 30 years has allowed for an almost routine deployment of various modeling techniques.^[1] In turn, they have become indispensable tools in modern materials science, offering fundamental insights into materials. Calculations neatly complement experiments either by a controlled manipulation of certain properties, by providing information beyond the experimental resolution, or by high-throughput search of novel materials with targeted features. For example, material response under extremely high pressures^[2] or restricted loading modes^[3,4] are hardly accessible experimentally, but rather straightforward to simulate. As other examples, it is possible to i) decouple chemical and elastic contributions to de-mixing enthalpies,^[5,6] ii) study separately, for example, polymorphic and ordering transformations, which are difficult to distinguish experimentally,^[7] iii) characterize metastable phases,^[8,9] iv) follow atomistic processes behind materials catastrophic failure,^[10] or v) learn about the chemistry at the very quantum-mechanical level.^[11,12] On the other hand, modern high-performance computer clusters make possible to perform a vast number of similar simulations,^[13] hence, probing the corresponding configurational space (being it, e.g., chemical composition, microstructure, or stress state), which would not be possible otherwise due to time and/or cost restrictions.

1.1. Multiscale/Multimethod Approach

Depending on a phenomenon of interest and/or a problem size, different experimental techniques are applied. For example, microstructural features at a millimeter scale can be studied by optical microscopy, at a micrometer scale by scanning electron microscopy (SEM), while features at a nanometer and subnanometer scale can be revealed by transmission electron microscopy (TEM) and atom probe tomography (APT). In a complete analogy to experiments, the problem under consideration, its size, available

computational resources, and an overall relation to experiment determine the most suitable modeling approach(es). A very detailed overview of available techniques can be found in ref.^[1]

Continuum mechanics is typically used for macroscale problems, for example, on the level of whole devices or real sample scales. Since this usually involves complicated geometries (e.g., edges of a drill bit), numerical solution using finite element method (FEM) is usually unavoidable. Microstructural developments can be addressed with quickly emerging phase field simulations. Mesoscale problems, such as a crack propagation or an evolution of dislocation networks rely mostly on the continuum description, however, involving also crucial regions (crack tips, dislocation cores), which have to be treated with the atomistic resolution. Here, two options are available for the description of atom-atom interactions: either using semi-empirical interatomic potentials, or by evaluating the electronic structure fully quantum-mechanically. The advantage of the former approach is its speed and capability of treating systems consisting of millions of atoms. Its disadvantage is that the final accuracy is determined by the quality and transferability of the employed interatomic potentials. (Classical) molecular dynamics ([C] MD), molecular statics (MS), and Monte Carlo (MC) methods are representatives of such atomistic techniques. On the other hand, quantum mechanical treatments, in the context of materials science most often within the Density Functional Theory (DFT),^[14,15] offer (in theory) a parameter-free description of interatomic interactions with the highest possible accuracy. However, their computational demands limit the system size to several dozens or hundreds of atoms. The principles and application of these atomistic methods are well introduced in a book by Lee.^[16]

All of these individual approaches are well developed, however, not a single of them represents a universally applicable tool. Consequently, many state-of-the-art developments are aiming on effectively combining these methods. A very prominent example of such activities is the modeling of dislocations.^[17] The dislocation core-region is described fully quantum-mechanically, near-core region is still treated with the atomic resolution, but using fast interatomic potentials, and finally the large scale interaction with other microstructural features is evaluated using continuum mechanics.

To give a better feeling for the above presented overview of methods and length scales, Figure 1 shows a zoom-in collage of a structure of a drill protected with a coating. It is interesting to realise, that while from the macroscopic point of view, the coatings are thin films (typically several hundreds of nanometers to a few microns thick), on the very atomistic level their characterization becomes essentially a bulk problem. This is of course true unless a finer structure, for example, superlattices with nanometer thin layers, exists or truly surface phenomena, for example, processes during growth, oxidation, etc., are involved.

The purpose of this paper is to provide an overview of our recent modeling activities, to demonstrate the diversity of

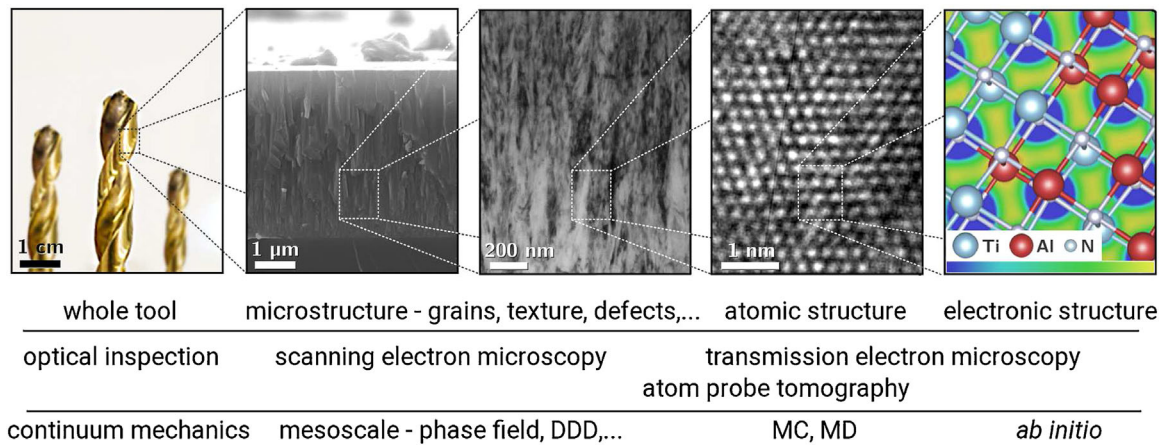


Fig. 1. A schematic picture demonstrating various material features, and experimental and modeling techniques used for their characterization, as a function of the length scale of interest.

phenomena and materials systems studied, as well as the strong interconnection between theory and experiment applied in our research. It is not the goal of this communication to provide an exhaustive overview on the many various developments pushing the borders of what is possible to model, but rather to demonstrate the applicability of existing and widely spread atomistic techniques to selected topics in the current materials science. This review mostly focuses on DFT “ab initio” calculations; some MC and MD-based simulations are presented in Section 5.

2. Computational Details

All “ab initio” results shown and discussed in this paper were obtained using the Vienna Ab initio Simulation Package (VASP),^[18–20] with the exception of the electron energy loss near edge structure (ELNES) calculations (Section 3.2), which were calculated with the Wien2k code,^[21] and several adsorption studies (Section 4.1), which were carried out using the OpenMX code.^[22,23] The exchange and correlation effects were treated in the majority of cases with the generalized gradient approximation (GGA), either parametrized by Wang and Perdew (PW91)^[24] or by Perdew, Burke, and Ernzerhof (PBE).^[25] For comparison purposes, in some parts also the local density approximation (LDA) was used. The reciprocal space was sampled with a Monkhorst-Pack grid.^[26] The number of k -points and the plane-wave cut-off energy were optimized to reach total energy accuracy in the range of a few meV at⁻¹. The bulk phases were always first fully relaxed, which includes energy minimization with respect to the unit cell volume, shape, and all atomic positions. Further optimizations depended on specific applications. For example, only atomic positions of an adatom in the direction perpendicular to the free surface were optimized for evaluation of the potential energy surface (Section 4.1). On the other hand, all atoms were kept fixed when calculating forces, which are used for a construction of the dynamical matrix in the (quasi-)harmonic approximation (QHA) to vibrational properties (Section 3.5). For specific details of each

calculation, the reader is referred to respective references given further in the text.

Structural and/or magnetic disorder was modeled within the special quasi-random structures (SQSs) methodology.^[27,28] It is a supercell based approach, in which the atoms are distributed over all sites so as to best mimic their distribution in a statistically random solid solution. Let us consider a binary alloy A_xB_{1-x} , in which every of N sites has M nearest neighbors. Let N_{AB} be a number of A–B bonds in a supercell with a certain distribution of xN A and $(1-x)N$ B atoms. In a random solid solution, the probability of a site being A-type is x . Out of its M neighbors, $(1-x)M$ are B-type. On the other hand, the probability that this site is occupied with an atom B is $(1-x)$. In that case, xM neighboring sites are A-type. Altogether, each site contributes with $x(1-x)M + (1-x)xM = 2x(1-x)M$ A–B bonds. Therefore, the total number of the A–B bonds per N sites is $x(1-x)MN$, where a factor 1/2 correcting for double-counting of each bond was applied. This allows to define a Warren-Cowley short range order (SRO) parameter^[29] as

$$\alpha = 1 - \frac{N_{AB}}{x(1-x)MN}. \quad (1)$$

$\alpha = 0$ suggests a statistically random solid solution, $\alpha > 0$ and $\alpha < 0$ correspond to a tendency for clustering and ordering, respectively. In practice, SRO parameters α_j for several coordination shells j are evaluated ($\alpha_2 = \alpha$ in Eq. 1), and as a criterion for selecting the best representing supercell is used.

$$\sum_j w_j |\alpha_j| \rightarrow \min, \quad (2)$$

where w_j are chosen weights, which should reflect effective strength of interaction in the system. Extensions of this formalism for ternary and multinary alloys have been also proposed.^[30–32] In some cases, also clusters beyond pairs, such as triplets, quadruplets, etc. should be considered. More technical details on efficient SQS generation and related parameters can be found in refs.^[33–35] In the case of quasi-

binary alloys, for example, $Zr_{1-x}Al_xN = (ZrN)_{1-x}(AlN)_x$, the SQS method is applied only to one sublattice. The SQS method has been also applied to construct a structural model for paramagnetic materials: a collinear spin up and spin down magnetic moments are distributed according to a binary SQS.^[36–38]

ELNES calculations were performed within a dipole approximation using the TELNES.3 package,^[39] distributed together with the Wien2k code. SC-EMA^[40–42] is a convenient on-line tool for postprocessing single-crystal elastic properties. Vibrational properties were calculated within QHA using a finite displacement method as implemented in the phonopy code,^[43,44] which works as a pre- and post-processor, for example, VASP calculations. Thermodynamic properties of the paramagnetic structures were calculated using the spin-space averaging (SSA) technique.^[37,45] VESTA software^[46] was used for a visual inspection of the structures.

The Monte Carlo simulations in Section 5 were carried out in an (NVT)-ensemble with a constant number of particles N , constant volume V , and constant temperature T . Positional updates were performed using a standard Metropolis algorithm that gives probability for accepting the position as $p = \exp(-\Delta E/k_B T)$,^[47] where ΔE denotes the difference in the total energy of the system before and after the displacement and k_B is the Boltzmann constant. Total energies E were evaluated using classical interatomic potentials.^[48,49] The molecular dynamics (MD) simulations of gold nanoparticles (Section 5) were performed using the LAMMPS package^[50] together with an interatomic potential describing the gold-gold interaction within the embedded atom method (EAM) as parametrized by Grochola, Russo, and Snook.^[51]

3. Bulk Materials

As mentioned already in the introduction, prediction of bulk properties is vital even for materials used as thin films. This section provides an overview of structural, electronic, mechanical, and thermal properties calculated for various material classes, and presents them in a context of available experimental data.

3.1. Phase Stability

Different levels of phase stability can be distinguished. Chemical stability is quantified by energy of formation, E_f . Here, negative value of E_f expresses an existence of a thermodynamic driving force for formation of the system from its individual constituents. On the other hand, a system is said to be in a statically (in the literature often termed also mechanically) stable state, when it corresponds to a local or global energy minimum in the Born-Oppenheimer configurational space, that is, its internal energy

increases for any (small) displacement of the atomic positions. The latter will be discussed later in Section 3.4, while here, we focus on the chemical stability.

The energy of formation reads

$$E_f = E_{\text{tot}} - \frac{1}{N} \sum_i N_i \mu_i, \quad (3)$$

where E_{tot} is the total energy (per atom) of the investigated phase, represented by an N -atomic (super)cell consisting of N_i atoms of a species i , $\sum_i N_i = N$, μ_i is a chemical potential of the species i , typically set equal to the total energy (per atom) of the ground state of the species i (e.g., fcc-Al, hcp-Ti, bcc-Mo, N_2 , O_2 , etc.).

Calculated energies of formation for quasi-binary ZrN–AlN system, in which the metal sublattice is a solid solution of Zr and Al atoms, are shown in Figure 2a. Since all E_f values are negative, they represent (meta)stable phases.^[6] The lowest energy of formation for ZrN is obtained for the rock-salt cubic structure (B1), while the wurtzite structure (B4) yields the lowest E_f value for AlN. Interestingly, intermediate compositions yield almost the same E_f values of the cubic B1 and another hexagonal structure, the B_k structure. This suggests a competition between these two phases, ultimately leading to a dual phase microstructure. And indeed, such compositionally induced structural evolution was experimentally observed.^[6,52–54] Similarly excellent agreement with the “ab initio” predicted phase composition has been reported also for other nitride systems.^[6,55–63]

The same data evaluated with $\mu_{Zr} = E_{\text{tot}}^{\text{hcp-Zr}} - 2.5\text{eV}$ (Figure 2b) represent Zr-poor conditions during the synthesis (caused, e.g., by a target poisoning during the sputter deposition). As one intuitively expects, the cubic Zr-deficient phase, Zr_3N_4 (Figure 2c) becomes likely to appear under such conditions.

Encouraged by the excellent agreement of these predictions with experiments, the same methodology was applied to another important protective coating system, namely quasi-binary Al_2O_3 – Cr_2O_3 . The ground state structure of both,

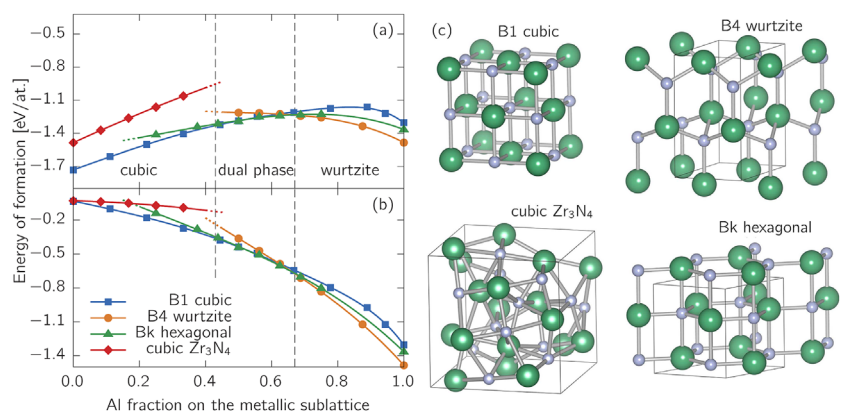


Fig. 2. The computed energy of formation, E_f , as a measure of the chemical phase stability, of the quasi-binary $(ZrN)_{1-x}(AlN)_x$ system evaluated in (a) Zr-rich and (b) Zr-poor conditions for four structural candidates pictured in panel (c). Total energies for the B1, B4, and B_k phases were taken from ref.^[6]

Al_2O_3 and Cr_2O_3 , is a hexagonal α structure, while a cubic defected B1-based structure and a defected spinel structure have been reported as metastable.^[64–66] There are also other phases in the Al–Cr–O phase diagram, but with only a little importance for the physical vapour deposited (PVD) Al_2O_3 – Cr_2O_3 coatings. The energy of formation based evaluation of phase stability, as well as the equilibrium phase diagram underpin this scenario, which is, however, in a strong disagreement with what is experimentally observed for PVD thin films.^[67,68] These are mostly cubic, recrystallize to the hexagonal α structure upon annealing at high temperatures of around 1200–1300 °C^[69] (sometimes even for lower temperatures), and remain hexagonal upon subsequent cooling to the room temperature. PVD is a process far from the thermodynamic equilibrium,^[70] and consequently a high number of point defects exists in the as-deposited state, which had been suggested to play an important role for the phase stability assessment.^[71,72] Therefore, we have investigated the relative changes of E_f for the α , γ , and B1-like phases containing vacancies, interstitials, Frenkel pairs, and Schottky defects.^[68] Most of these point defects, when present, decrease the energy difference between the hexagonal and the cubic phases, hence, making the latter less unfavourable. This effect is strongest for O Frenkel defects, which even turn the cubic γ phase to be energetically more preferable than the α structure. Moreover, analysis of the Frenkel defects formation energy clearly shows that O (and Al) Frenkel pairs are energetically less expensive to form in the γ than in the α -phase, irrespective of the distance between the interstitial atom and the vacancy (Figure 3), hence, making O Frenkel pair a possible γ -stabilizer.

Despite the scenario presented above is greatly oversimplified with respect to reality, it clearly demonstrates how important is the role of point defects unavoidably present in PVD-synthesized materials. In this light, the excellent agreement between the phase stability predictions of (perfect) nitrides and experimental observations on PVD coatings becomes somewhat surprising. Euchner and Mayrhofer^[73] have recently performed a study on the influence of vacancy content on the phase stability of $\text{Ti}_{1-x}\text{Al}_x\text{N}$. They concluded that up to a vacancy content of a few atomic percent, no significant shift of the cross-over between E_f of the cubic and wurtzite phases occurs, although E_f values of individual phases, of course, change. It, therefore, remains to be checked whether $\text{Ti}_{1-x}\text{Al}_x\text{N}$ is only “a lucky textbook case”, or whether phase stability is insensitive to the vacancy content also for other nitride systems (as seems to be the case based on the good agreement between theory and experiment). In the latter case, the possible explanation of this dramatically different behavior may originate in the structural simplicity of nitrides in contrast to the complicated structure of oxides. Incorporation of oxygen in $\text{Ti}_{1-x}\text{Al}_x\text{N}$ leads to formation of metal vacancies, hence, making their treatment in theoretical models indispensable.^[74–76]

Arguments based on the energy of formation used to support experimental observations of often puzzling phase composition have been also applied to elucidate, for example, Si partitioning in TiAl intermetallics,^[77] O-vacancy clustering in iron^[78] or Fe atoms in Fe–Ti alloys,^[79] to corroborate atom probe data of carbides in a Hf–Mo–C alloy,^[80] to rationalize structure and mechanical properties of oxynitrides,^[75,76,81] or to study borides,^[82,83] a novel perspective class for hard coating applications.

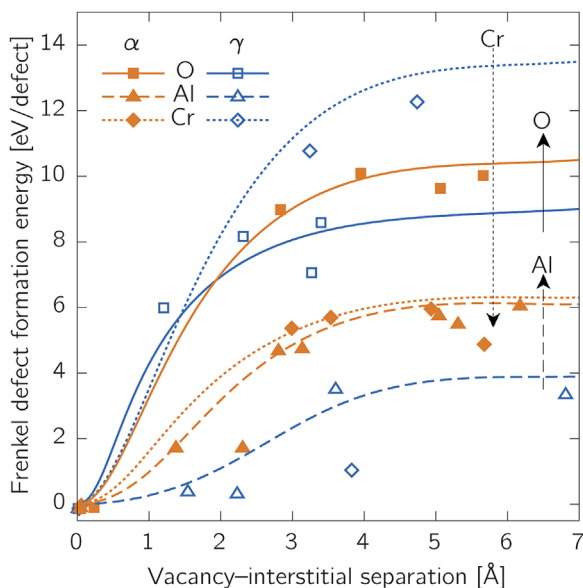


Fig. 3. Calculated defect formation energy for Al (triangles, dashed lines), Cr (diamonds, dotted lines), and O (squares, solid lines) Frenkel pairs in γ - (blue symbols) and α - (orange symbols) $(\text{Al}_{0.69}\text{Cr}_{0.31})_2\text{O}_3$ as a function of the vacancy-interstitial separation. The lines are only guides for the eyes. The large separation limits are data presented in ref.^[68]

3.2. Electronic Structure

The essential quantity calculated by DFT is a distribution of the electron charge density. Thereby, information on the electronic structure (e.g., band gap, density of states, band structure, bonding) is promptly available. The calculated electronic structure is usually compared with experiment indirectly, for example, by optical properties (refractive index, complex dielectric function, see, e.g., ref.^[84]) or by electron energy loss spectroscopy (EELS), which is an analytical technique performed in TEM. Intensity of its subset, electron energy loss near edge structure (ELNES), is in the first approximation proportional to the density of unoccupied states corresponding to the final state of the excitation process, for example, N- p states for the K-edge ($1s \rightarrow 2p$ transition). The calculated compositional evolution for $\text{Al}_{1-x}\text{Ga}_x\text{N}$ and $\text{Ti}_{1-x}\text{Al}_x\text{N}$ showed excellent agreement with the measured spectra.^[85] In the latter case, ELNES is also capable of picking the structural evolution (cubic to wurtzite) with increasing AlN mole fraction in $\text{Ti}_{1-x}\text{Al}_x\text{N}$.^[6,86] Analysis of the “ab initio” calculations revealed the origin of individual peaks, that is, that the first peaks above the edge onset originate from the Ti–N hybridized anti-bonding states.

Recently, Zhang et al.^[87] measured variations of the N K-edge ELNES of CrN with N off-stoichiometry, and the authors speculated on presence of N vacancies.^[87,88] We employed DFT calculations of paramagnetic CrN to confirm this hypothesis. Both, calculated and measured N K-edge ELNES (Figure 4) show decrease of the intensity of the second peak (at about 12 eV above the edge onset), hence, confirming the feasibility of the proposed scenario.

3.3. Elasticity

A very successful and well developed application of the first principles calculations is the prediction of elastic properties. The most straightforward method is a direct application of the Hooke's law within the linear elasticity (so called stress-strain method),

$$\sigma_i = \sum_j C_{ij} \varepsilon_j, \quad (4)$$

where σ_i and ε_j are components of the stress and the strain vectors, respectively. They are related to the components of the second-order stress (σ_{kl}) and strain (ε_{kl}) tensors using the Voigt's notation:

$$c|*6ci123456 \uparrow\uparrow\uparrow\uparrow\uparrow\uparrow (k,l)(1,1)(2,2)(3,3)(2,3), (3,2)(1,3), (3,1) (1,2), (2,1) \quad (5)$$

C_{ij} is a 6×6 symmetrical matrix of elastic constants (or stiffnesses); the (i, j) component of the C_{ij} matrix corresponds to the (k, l, m, n) component c_{klmn} of the fourth rank elasticity tensor, $i \leftrightarrow (k, l), j \leftrightarrow (m, n)$. The inverse Hooke's law relating strain to stress, employs compliances, s_{klmn} , instead of elastic constants, c_{klmn} . Here, the Voigt's notation becomes extremely useful as the the 6×6 matrix of compliances, S_{ij} , is simply an

inverse matrix of the 6×6 elastic constants matrix, C_{ij} . Note, that the relationship between the two indices (i, j) of the compliance matrix, and four indices (k, l, m, n) of the compliance tensor is not as straightforward as in the case of elastic constants.^[89]

The stress-strains method is a very efficient since, in principle, it requires only six calculations for six specially designed strains (deformations), which, in turn, allow to establish all 21 independent components C_{ij} .^[90,91] In practice, more calculations are desirable in order to eliminate effects of a not perfectly relaxed initial state (which has the accuracy of $O(\sigma^2)$ when the total energy minimization is applied), as well as to make sure one applies large enough deformations to minimize numerical errors, but small enough to stay in the linear elasticity regime. If the stress vector σ_i is not available, it is always possible to extract the elastic constants using energy-strain method,^[92-95] in which the difference between total energy in a deformed state, $E_{tot}(\varepsilon_i)$, and in equilibrium, $E_{tot}(0)$, is assigned to the elastic strain energy.

$$E_{tot}(\varepsilon_i) - E_{tot}(0) = \frac{1}{2} V \sum_{ij} C_{ij} \varepsilon_i \varepsilon_j. \quad (6)$$

V is equilibrium volume of the simulation cell. It is convenient to apply specially selected deformation modes, which result in simple (quadratic) functional dependences in Equation 6. Although this method is computationally more demanding, as it requires more calculations to obtain enough datapoints for the quadratic fitting, it allows to pick up also non-quadratic (i.e., beyond linear-elasticity) effects in a straightforward manner and, thus, to establish, for example, third order elastic constants, C_{ijk} .^[92-94,96] Even more importantly, in the most recent studies this method has been used to establish also temperature dependence of the elastic constants.^[97-99] It is also worth mentioning that, if all parameters are carefully chosen, both stress-strain and energy-strain approaches yield the same results (as they should, since both are based on the Hooke's law and linear elasticity).^[91,100] Again, the SQS methodology has proved to be useful for predicting compositional trends of solid solutions, as well as to treat the magnetic disorder in paramagnetic CrN-based systems.^[34,37,99-104]

For practical reasons, the resulting elastic data are often processed to yield quantities more relevant for experiments dealing with polycrystalline materials.^[40,94,103,105] Holec et al.^[103] explicitly showed the impact of texture and preferred orientation of $Zr_{1-x}Al_xN$ solid solutions on the value of directionally dependent Young's modulus, E_{hkl} . By definition, Young's modulus relates uniaxial stress with strain induced in the same direction and, hence, for elastically anisotropic materials varies with the direction of loading. For example, variations in texture may result to Young's moduli values ranging from 350 to 470 GPa for pure ZrN with the (100) fibre texture.^[103] Therefore, in any comparison with experiment, the particular microstructure should be carefully considered.

Young's modulus of $Zr_{1-x}Al_xN$ is independent of the texture for $x \approx 0.5$.^[103] Hence, at this composition, its

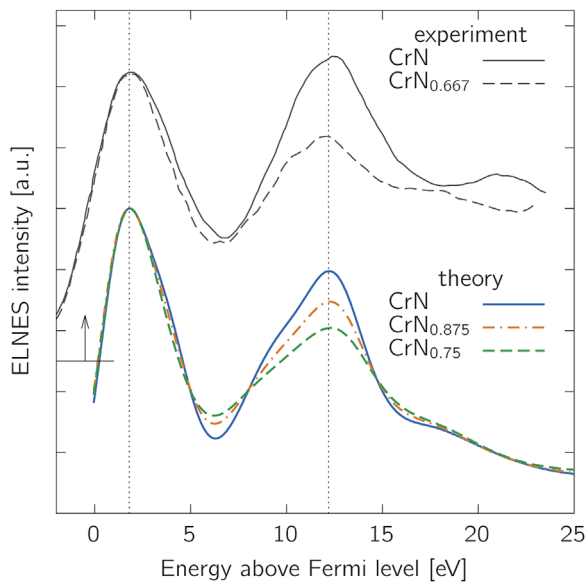


Fig. 4. Calculated and experimentally measured nitrogen K-edge ELNES of CrN_x . The experimental data are taken from ref.^[87]

mechanical response does not depend on a particular microstructure as long as the contribution of grain boundaries can be neglected.^[103] Recalling Figure 2, however, we see that a dual phase microstructure, composed of cubic and hexagonal structures, is predicted (and observed^[6,52]) for $x \approx 0.5$. Therefore, we have calculated also elastic properties of the hexagonal wurtzite-like phase. The Voigt (constant strain over all grains, upper bound) and Reuss (constant stress over all grains, lower bound) limits of Young's and shear moduli for polycrystalline aggregates with no texture are related to the single crystal elastic constants, C_{ij} , and compliances, S_{ij} , via^[106]

$$E_V^{\text{cub}} = \frac{(C_{11} - C_{12} + 3C_{44})(C_{11} + 2C_{12})}{2C_{11} + 3C_{12} + C_{44}} \quad (7)$$

$$E_R^{\text{cub}} = \frac{5}{3S_{11} + 2S_{12} + S_{44}} \quad (8)$$

$$G_V^{\text{cub}} = \frac{C_{11} - C_{12} + 3C_{44}}{5} \quad (9)$$

$$G_R^{\text{cub}} = \frac{5}{4S_{11} - 4S_{12} + 3S_{44}} \quad (10)$$

hexagonal:

$$E_V^{\text{hex}} = \frac{(7C_{11} + 2C_{33} - 5C_{12} - 4C_{13} + 12C_{44})(2C_{11} + C_{33} + 2C_{12} + 4C_{13})}{3(9C_{11} + 4C_{33} + 5C_{12} + 12C_{13} + 4C_{44})} \quad (11)$$

$$E_R^{\text{hex}} = \frac{15}{8S_{11} + 3S_{33} + 4S_{13} + 2S_{44}} \quad (12)$$

$$G_V^{\text{hex}} = \frac{7C_{11} + 2C_{33} - 5C_{12} - 4C_{13} + 12C_{44}}{30} \quad (13)$$

$$G_R^{\text{hex}} = \frac{15}{14S_{11} + 4S_{33} - 10S_{12} - 8S_{13} + 6S_{44}} \quad (14)$$

The results are visualised in Figure 5a and b, together with their corresponding Hill's averages (e.g., $E_H^{\text{cub}} = (E_R^{\text{cub}} + E_V^{\text{cub}})/2$). Interestingly, the most isotropic response of the hexagonal phase is predicted for $x \approx 0.8$, which is significantly more than for the cubic phase ($x \approx 0.5$). This is well documented by a vanishing spread of the Voigt and Reuss limits of Young's and shear moduli (Figure 5a and b) and further supported by a rather spherical distribution of directionally dependent (single crystal) Young's modulus for $x = 0.875$ as shown in Figure 6. Ratio of bulk and shear moduli, B/G , is often used as an

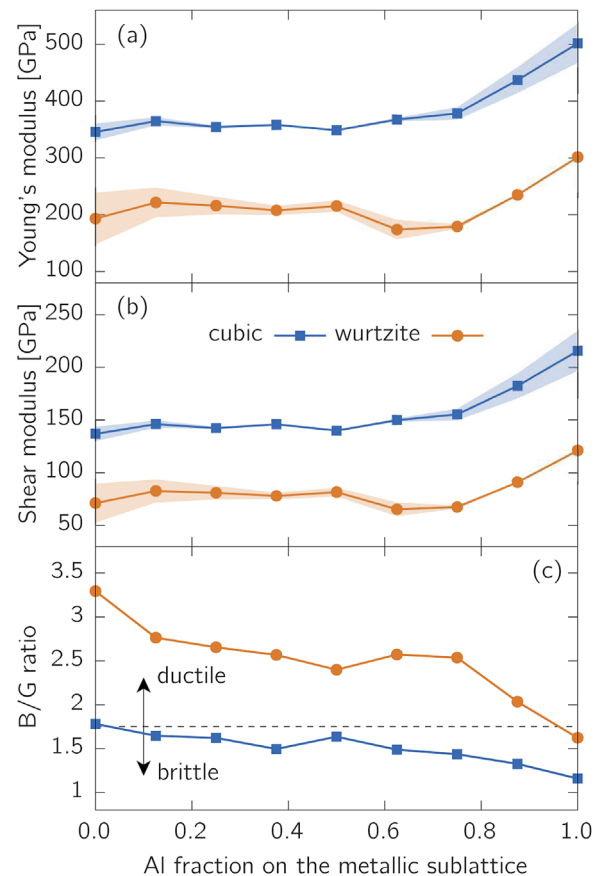


Fig. 5. Calculated elastic properties, (a) Young's, E , and (b) shear, G , moduli of isotropic polycrystalline aggregates of cubic (blue, squares), and hexagonal (orange, circles) phases of $Zr_{1-x}Al_xN$. The actual values represent Hill's averages, while the shaded areas demonstrate spread between Reuss and Voigt limits. (c) Pugh's B/G criterion for characterizing ductile versus brittle behavior. The data for the cubic phase are taken from ref.^[103]

indicator for ductile or brittle behavior.^[107] In this respect it is very interesting to note that, while both Young's and shear moduli are lower for the hexagonal phase than for the cubic one, the B/G ratio is higher for the hexagonal structure for all compositions, hence, suggesting that the hexagonal phase in the dual phase microstructure improves ductility of this ceramic system.

Finally, we note that although single phase polycrystalline $ZrAlN$ with an isotropic elastic response is unlikely to exist, a similar prediction has been obtained also for $Ti_{1-x}Al_xN$ for $x \approx 0.3$,^[101] for which single-phase cubic structure is obtained also experimentally.^[6,108]

Directionally dependent Young's modulus can be considered as a first approximation beyond the isotropic elasticity to the elastic response during nanoindentation loading, although the real mechanical response involves complicated plastic and elastic deformations,^[109] with stress fields being far from a simple uni-axial loading mode. In our recent study, we compared the nanoindentation elastic modulus of $Cr_{1-x}Mo_xN$ with the directionally dependent Young's modulus predicted by "ab initio."^[104] An acceptable agreement was obtained for the Young's modulus in the $\langle 100 \rangle$

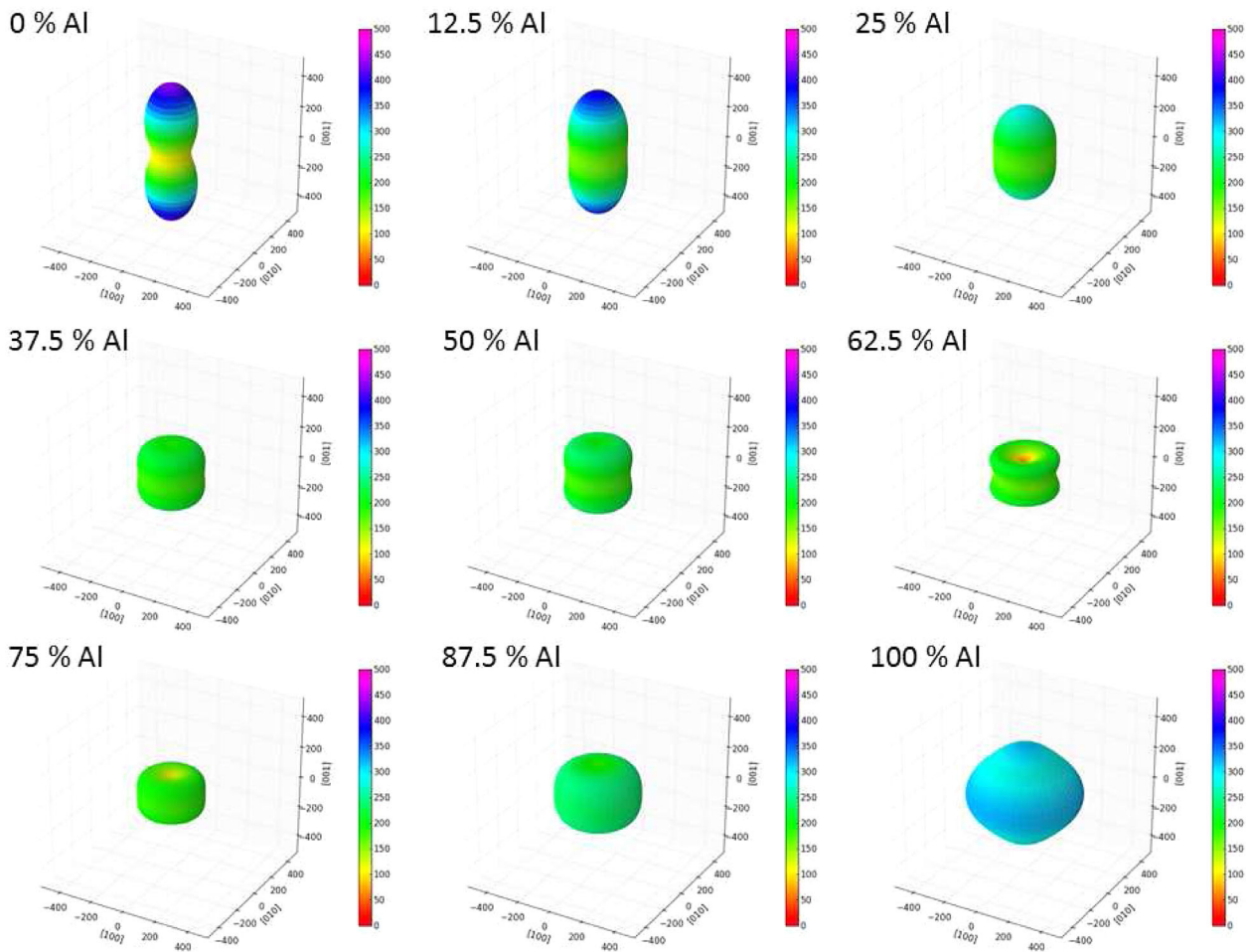


Fig. 6. Directionally dependent Young's modulus for the single crystal hexagonal (wurtzite-like) $Zr_{1-x}Al_xN$. The distribution most similar to a sphere, and hence, closest to elastic behavior, is predicted for AlN mole fraction of 0.875. The visualization was done using the SC-EMA tool (<http://scema.mpie.de/>).

direction, which was the preferred grain orientation as revealed by X-ray diffraction (XRD).^[110] These data were compared also with earlier published observations for the same coating system, but with a preferred orientation along the $\langle 111 \rangle$ direction. In this case, the indentation moduli were lower and exhibited a perfect resemblance with the calculated Young's modulus in the $\langle 111 \rangle$ direction.

3.4. Statical Stability

Elastic constants are also indicators of statical stability: for a given equilibrium of a system to be statically stable, all (small) perturbations must increase its total energy (equilibrium internal energy plus elastic strain energy), hence, creating a force returning the structure back to equilibrium. Depending on the crystal symmetry, different inequalities involving elastic constants, called Born–Huang stability criteria,^[111,112] have to be fulfilled. This is an important part of a (meta) stability assessment of a given system. For example, although β_o -TiAl having an ordered B2 structure has lower energy of formation, E_f , than β -TiAl, which is a disordered bcc phase, the β_o phase is statically unstable at 0 K. The “ab initio”

calculated elastic constants $C_{11} = 82\text{GPa}$, $C_{12} = 127\text{GPa}$, and $C_{44} = 68\text{GPa}$ do not fulfil $C_{11} > |C_{12}|$, which is one of the Born–Huang stability criteria for cubic materials.^[112] Contrarily, the elastic constants of β -TiAl ($C_{11} = 115\text{GPa}$, $C_{12} = 102\text{GPa}$, $C_{44} = 84\text{GPa}$) do fulfil all stability conditions,^[113] and, hence, the disordered configuration is a potential metastable phase.

With an increasing amount x of Mo substituting for Al in $TiAl_{1-x}Mo_x$ (since Mo preferentially occupies Al the sublattice,^[114]) the ordered phase is also stabilized.^[113] This is in agreement with a well known fact, that Mo acts as so-called β -stabilizer,^[115] and the ordered phase appears also in the equilibrium ternary Ti–Al–Mo phase diagram.^[116] Nevertheless, even the fulfilment of the Born–Huang stability criteria does not guarantee a phase to be (meta)stable. A structure may still be unstable with respect to displacements of atoms inside the unit cell, that is, it corresponds to a saddle point or (local) maximum in Born–Oppenheimer configurational space. Such instability is indicated by purely imaginary values of some vibrational frequencies (soft phonon modes) away from the Γ point, and is, hereafter, called phonon or vibrational instability (in the literature also

often termed as dynamical instability). The Γ point itself corresponds to long-wavelength limit vibrational modes, that is, to elastic waves covered by the Born–Huang stability criteria. Once again using the example of the TiAl + Mo system, although $\approx 5\text{at}\%$ of Mo stabilises the ordered β_0 structure with respect to unit cell deformation, it still remains vibrationally unstable (though much less than in the case without Mo).^[113] CrN^[37] is another example, in which fulfilment of the Born–Huang stability criteria does not guarantee the full statical (meta)stability of a particular system.

There is a very close connection between statical stability of materials and their theoretical (ideal) strength, which sets the stability limits of materials under various external loading conditions. Of course, in most engineering applications, the strength of materials is controlled by nucleation and motion of dislocations or microcracks. If such defects were not present, the mechanically loaded material would only fail at much higher stresses, comparable with the Young’s modulus of the material. Such a stress for a particular loading or deformation is called theoretical or ideal strength and it is an upper limit of stresses attainable prior to failure at the deformation mode applied. It is a measure of the strength of bonds in materials and provides more insight into their structure and properties. In addition to that, there are more and more applications of defect-free materials in today’s technology, where theoretical strength may be approached and, therefore, its reliable knowledge is crucial. A very recent review of this topic may be found in ref.^[117] reviews of previous activities in this field and the connections with displacive phase transformations are given in refs.^[118–120] If, however another instability (due to, e.g., soft phonon modes, magnetic spin arrangement, etc.) occurs prior to reaching the stress corresponding to the ideal strength, then this lower stress sets the theoretical strength of the material.^[10,121,122]

3.5. Ab Initio Thermodynamics

Density Functional Theory is a ground state theory and, thus, within its original formulation allows accessing materials properties – first of all – at 0 K. However, in particular within the last decade, new methodologies have emerged which advanced DFT simulations to finite temperatures (for more details see, e.g., reviews by Palumbo et al.^[123] or Baroni et al.^[124]). One prerequisite in doing so has been the development of computationally efficient methods enabling to perform highly-accurate lattice dynamics simulations.^[125–127] A genuine challenge occurring for magnetic materials is the inclusion of magnetic excitations (for recent reviews we refer to, e.g.,^[128,129]), in particular the proper treatment of spin quantization,^[130–133] as well as the interplay between lattice and magnetic excitations (see, e.g.,^[37,45,134–136]).

Such techniques enable nowadays fully parameter-free and highly-accurate material properties predictions, for example, for specific heat capacities of steels^[129,137,138] or complex multi-component alloys.^[139–141] A prerequisite for deriving

such thermodynamic materials properties is the computation of the Helmholtz free energy, $F(T, V)$, which is given in the adiabatic approximation as

$$F(T, V) = E(V) + F_{\text{el}}(V, T) + F_{\text{vib}}(V, T) + F_{\text{mag}}(V, T) + F_{\text{conf}}(V, T) + \dots, \quad (15)$$

and which is related to the Gibbs energy, $G(T, p)$, via a Legendre transformation between p and V . In above equation, $E(V)$ is the internal energy (total energy) at 0K, and F_{el} , F_{vib} , F_{mag} , and F_{conf} are free energy contributions related to electronic excitations, lattice vibrations, magnetic excitations and chemical disorder. The latter free energy contribution vanishes for ordered compounds (see, e.g.,^[142] for a recent overview).

The typically largest free energy contribution in Equation 15 is given by F_{vib} , that is, by the lattice vibrations.^[143,144] A widely employed and efficient method to compute F_{vib} is the so-called quasi-harmonic approximation (QHA), in which phonon computations are carried out at a series of volumes, thus, taking thermal lattice expansion into account.^[143] Note that even though the individual free energy contributions are adiabatically decoupled in Equation 15, they can still depend on each other. For instance, even though magnetic fluctuations are usually fast compared to atomic motion,^[145] at a given temperature the underlying interatomic forces (and hence vibrations) in magnetic materials can still depend on the actual magnetic state^[45,134] (see also discussion below). It must be also noted that there exists a number of systems, which are vibrationally unstable at 0K, but exist at finite temperatures due to anharmonic and/or entropic stabilizing effects. In such cases, it becomes necessary to employ advanced methods beyond the QHA, for example, the self-consistent “ab initio” lattice dynamical (SCAILD) method,^[146–148] the up-sampled thermodynamic integration using Langevin dynamics (UP-TILD) method,^[125,126] approaches based on “ab initio” molecular dynamics runs,^[149,150] the temperature-dependent effective potential (TDEP) method,^[38] the large displacement finite-difference (LDFD) method,^[150] or the stochastic self-consistent harmonic approximation (SSCHA).^[151]

Once the Helmholtz free energy or Gibbs energy is derived, thermodynamic properties, such as the specific heat capacity at constant pressure, $C_p(T)$, volume and lattice constant expansion, $V(T)$ and $a(T)$, or their derivatives, the thermal volume/linear expansion coefficient (TEC), $\alpha_V(T)/\alpha(T)$, can be obtained via common thermodynamic relations. For cubic materials, $\alpha(T) = \frac{1}{3}\alpha_V(T)$. The TEC usually represents a very sensitive material property and provides, therewith, a good measure of the predictive power of the underlying computational model.

In the upper panel of Figure 7, the computed TECs of several binary early transition metal nitrides (TMNs) based on the quasi-harmonic approximation are summarized. It follows that TECs increases with decreasing valence electron concentration (VEC), correlated with lowering E_f ^[94,152] and, hence, presumably strengthening force constants. For

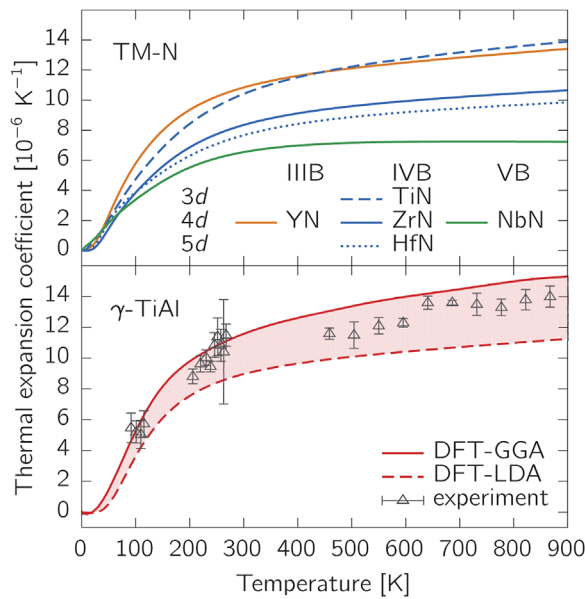


Fig. 7. Calculated lattice thermal expansion coefficient, $\alpha(T)$, for (a) a series of binary TMNs, and (b) intermetallic γ -TiAl (adapted from ref.^[159]). In the latter case, both GGA and LDA exchange-correlation potentials were used to get upper and lower limits framing the experimental data.

isovalent materials, group IVB-nitrides, TEC decreases from 3 to 4 to 5d elements. This is consistent with the Debye theory, in which the expansion coefficient is inversely proportional to the bulk modulus.^[153]

The lower panel of Figure 7 shows a comparison of calculated (based on the QHA) and experimental TEC for γ -TiAl. Note that the $L1_0$ structure is slightly tetragonal, however, the c/a ratio is close to 1. Such a slight tetragonality is hard to identify employing standard XRD techniques for the experimental determination of the TEC,^[154] and hence, we treat the structure as cubic. The quasi-harmonic calculations were done employing two commonly applied approximations for the xc-functional, namely the GGA-PBE and LDA exchange-correlation potentials providing the red solid and red dashed lines shown in Figure 7 (lower panel). The experimental data lie in-between the predicted TECs, which can be related to the fact that LDA (lower bound) typically overestimates the interatomic binding, while GGA (upper bound) underestimates it.^[143,155,156] Consequently, LDA (GGA) predicts stiffer (softer) material response resulting in underestimated (overestimated) TEC with respect to experiment. Both functionals provide a sort of confidence interval, similarly to a previous analysis of a large range of simple metals.^[143] A similar good agreement between theory and experiment was also obtained for paramagnetic CrN^[37] or metastable c-AlN.^[9] In the latter case, the situation is complicated by the fact that AlN is metastable in the NaCl cubic structure, and is stabilized only by a superlattice structure. Consequently, the experimental measurement had to be combined with an inverse problem modeling on the continuum level, in order to extract TEC for comparison with the “ab initio” predictions.

Gibbs energies are also basis for constructing phase diagrams, which provide the information of which phases are thermodynamically stable (at a given T and p) and allowing to identify phase transformations (e.g., via the cross-over of Gibbs energies for two different phases). The latter was used to establish the magneto-structural transition temperature of CrN. In CrN, the magnetic transition at the Néel temperature, T_N , coincides with a structural transition from the high temperature paramagnetic phase (cubic NaCl structure) to a low temperature anti-ferromagnetic phase (orthorhombic structure). As discussed above, the inclusion of magnetic excitations and their impact on vibrational properties for magnetic materials such as CrN is crucial. The latter can be incorporated, for example, via the spin-space averaging (SSA) technique.^[45] Taking the magnetic contributions properly into account, the standard GGA approximation yielded $T_N = 428\text{K}$. Note that for strongly correlated materials such as CrN, a standard GGA approximation turns out to be insufficient. As discussed in ref.,^[36] this could be overcome by employing the GGA + U approximation for CrN, that is, by adding a strong on-site Coulomb interaction. In fact, the GGA + U predicted temperature is $T_N = 300\text{K}$,^[37] being close to the experimentally reported value of 280K. A similar achievement was also reported by Shulumba et al. using the TDEP method for computing vibrations in paramagnetic materials.^[38]

These results demonstrate the predictive power of current theoretical approaches, which can be applied to many systems of practical interest, in particular in light of the nowadays available and ongoing increasing computational power. Advancements beyond the above described approximations are being developed, for example, to treat defected and/or disordered systems (e.g., to account at elevated temperatures for thermodynamically driven creation of vacancies^[126,144,157] or temperature-driven partitioning of substitutionally alloyed steels^[158]), the delicate interplay between various magnetic excitations (e.g., longitudinal spin fluctuations) and lattice vibrations (e.g., explicit anharmonic contributions)^[135,136] or for predictions in multi-component systems, such as the new class of high entropy alloys.^[140,141,159,160] An important application field for “ab initio” thermodynamic data is using them as input for the CALPHAD method^[161–166] implemented in simulation packages, such as Thermocalc^[167] and Matcalc.^[168] Latest advances in this direction have been summarized in a series of review papers.^[142,169–173] A recently developed TNM alloy,^[174,175] which is already in service, proves CALPHAD as a useful design tool for novel advanced structural materials with targeted microstructures.

4. Surface Phenomena

4.1. Surface Adsorption

Although many properties even of thin films are related directly to their bulk behavior discussed above, there are certain phenomena, which require the surface to be explicitly

included, for example, adsorption energy, adsorption sites and potential energy surface for surface adsorption. The adsorption energy, E_{ads} , of an adatom is defined as

$$E_{\text{ads}} = E_{\text{slab}+X} - (E_{\text{slab}} + \mu(X)), \quad (16)$$

where $E_{\text{slab}+X}$ and E_{slab} are total energies of a surface supercell with and without the surface adatom X , and $\mu(X)$ is the chemical potential of an isolated X atom. A negative value of E_{ads} suggests adsorption, while a positive value means that the atom X is repelled by the free surface.

In our recent studies, we used E_{ads} to establish whether various water-related species stick to different coating materials exhibiting low friction effect when tested in humid atmospheres. For example, we could show that both H and O physisorb on CrN(100) and TiN(100) surfaces, nevertheless a more negative value of E_{ads} is obtained for CrN.^[176] The preferred adsorption sites for H are in both cases above metal atoms, while O preferably sits above N sites on the CrN(100) surface and near (but not above) Ti sites on the TiN(100) surface. Potential energy surface (PES), which is E_{ads} as a function of the lateral position, provides an idea about preferred surface diffusion pathways and energy barriers. It turned out that the lowest energy barrier pathway for O is along the $\langle 100 \rangle$ direction on both materials. On the other hand, for H this direction is preferred only on the CrN(100), while H migrates along the $\langle 110 \rangle$ directions on the TiN(100) surface. Even more importantly, the surface diffusion barrier is about 0.8 eV for H on both systems as well as for O on CrN, while O atom on the TiN(100) surface experiences barrier of only about 0.5 eV. This lead us to propose a self-assembled nanobearing effect exhibited by TiN/CrN superlattices with small bi-layer periods,^[176,177] which relies on an accumulation of O (and possibly also other water-based species) on CrN (stronger bonded and less mobile than on TiN).

Similarly, low friction was measured experimentally also for Si-containing amorphous carbon (a-C:Si) coatings when tested in atmospheres containing humidity.^[178,179] It had been reported that the material in a tribological contact is in a strongly graphitized condition^[180] and, therefore, we calculated PES of H, O, OH- and H₂O physisorbed on graphene containing one Si atom.^[179] The “ab initio” calculations clearly indicated that all these species preferentially bind to Si; we have, therefore, speculated that Si attracts them and consequently initiates humidity-related nanobearing effect similarly to the CrN/TiN superlattice.^[176,177] This scenario was confirmed by an XPS analysis, which revealed a high amount of Si-O bonds.^[179]

An unusual effect was predicted for adsorption of O₂ and other environmental gasses, such as H₂O, on Ti_{0.5}Al_{0.5}N(100).^[181] As Al₂O₃ is more stable than TiO₂, a common intuition is that oxidation of Ti_{0.5}Al_{0.5}N is dominated by Al-O interactions. However, we predicted Ti sites to be preferred in the early stages of oxidation.^[181] This DFT result was also validated experimentally.^[182] In practice, certainly other environments or workpieces can

be interacting with Ti_{1-x}Al_xN and other hard coatings in applications. One such example is extrusion of polymers. To protect steel extruders from polymers, they need to be coated. Ti_{1-x}Al_xN does not interact strongly with polypropylene unless radicals are formed in the melt,^[183] making it suitable for these applications. Clearly, environmental interactions must be included in DFT studies to achieve more realistic predictions.

4.2. Implantation of Point Defects

Adsorption energy turned out to be inappropriate for ranking coatings for forming tool application aiming at improved resistivity against material transfer during the contact.^[184] This is because the material transfer during the forming process happens under high applied load, in contrast to the external load-free condition valid for evaluation of E_{ads} . Therefore, an alternative ranking based on implantation of an atom inside the material, was proposed.^[184]

Let $E_{\text{slab}+X}(d)$ be the total energy of a slab with an adatom X , as a function of the distance d between the adatom and the free surface. Implantation potential, $U(d)$, is defined as

$$U(d) = E_{\text{slab}+X}(d) - (E_{\text{slab}} + \mu(X)), \quad (17)$$

where E_{slab} is the total energy of the slab without the adatom, and $\mu(X)$ is the energy of an isolated adatom atom X . Obviously, $U(d) = 0$ for $d \rightarrow \infty$, and a local minimum for $0 < d < \infty$ corresponds to E_{ads} at that site. An example of $U(d)$ for Al implantation into TiN and Ti_{0.5}Al_{0.5}N is given in Figure 8 (the minimum corresponding to E_{ads} is reached for $d \approx 2 \text{ \AA}$). The repulsive/attractive force, $F = -\partial U(d)/\partial d$, between an adatom and the slab is zero at the equilibrium adsorption distance, it is attractive for larger d and repulsive

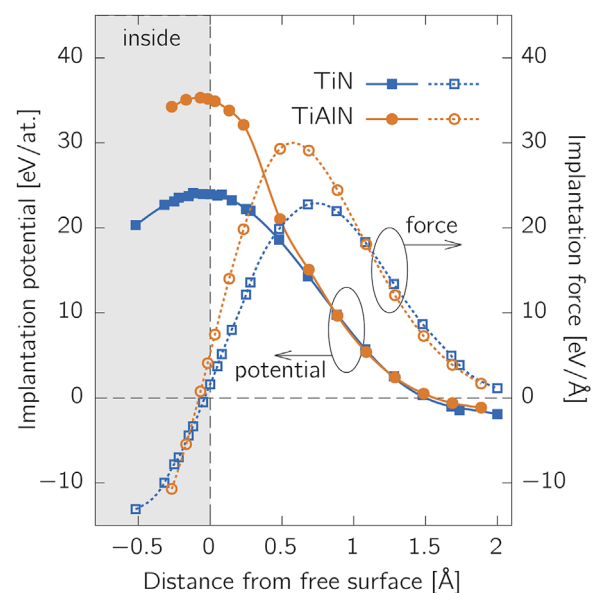


Fig. 8. Implantation barrier, $U(d)$ (Eq. 17), and implantation force, $F = -\partial U(d)/\partial d$, for Al adatom implanted into TiN (blue squares) and Ti_{0.5}Al_{0.5}N (orange circles) through the hollow site on the (100) surface.

for smaller distances d . However, when the distance becomes negative, that is, the adatom is implanted inside the material, the force changes again its sign (direction) and pulls the adatom into the nearest interstitial position. Hence, the $F = 0$ at $d = 0$, and reaches its maximum, hereafter, called the implantation force, at the inflexion point of $U(d)$. We note that the slight offset in d for $\text{Ti}_{0.5}\text{Al}_{0.5}\text{N}$ (Figure 8, orange curve) is related to the local relaxations of the surface atoms. On the other hand, the height of the implantation barrier, that is, the maximum of $U(d)$ reached at $d = 0$ is an indicator of the minimum kinetic energy that an incoming atom must have in order to penetrate (as an interstitial atom) into the material during, for example, PVD deposition. From Figure 8 is clear that pure TiN is more prone to Al interstitials than $\text{Ti}_{0.5}\text{Al}_{0.5}\text{N}$.

5. Nanoparticles

Systems with a broken periodicity, represent an increased difficulty when handled with codes relying on periodic boundary conditions (PBC) as is the case of, for example, VASP or Wien2k. The application of PBC implies a regular arrangement of the simulation boxes. Therefore, even a simple calculation of “bulk” graphene containing two atoms in its unit cell, which is periodically repeating in-plane, hence creating a 2D crystal, involves a stack of planar graphene sheets. The separating vacuum must be thick enough to avoid (or minimize) any interaction between the individual sheets, artificially introduced by the PBC. Similarly, nanotubes require vacuum separation in 2D, while 3D molecules and nanoparticles must be separated in all three directions.

Although the current computational resources allow for modeling of such objects directly with the first principles methods, it is often desirable to combine them with atomistic simulations (molecular dynamics or Monte Carlo) due to a large number of atoms involved, which becomes impractical for “ab initio.”

5.1. Excess Energy

Carbon-based nanostructures are a fascinating class of materials, which has drawn much attention in particular after the 2010 Nobel Prize in Physics was awarded to Andre Geim and Konstantin Novoselov for their experimental work on graphene. Although planar graphene is the most simple carbon nanostructure, the interpretation of corresponding simulation results is far from trivial. This is due to the “Yakobson paradox” meaning that the apparent thickness of graphene may differ more than order of magnitude depending on the type of simulation performed.^[185–187] In curved nanostructures, such as carbon nanotubes and fullerenes, the curvature induced excess surface energy enters as a new parameter characterizing the material. It is the determination of the excess surface energy of the double curved, spherical fullerenes that this review focuses on in the following. A quest to characterize curvature-induced excess energy of carbon fullerenes by “ab initio” quickly hit the limits with respect to

the molecule size: apart from the smallest fullerene C_{60} , only C_{70} , C_{180} , and C_{240} could be reasonably calculated, thereby, not even reaching a radius of 1nm.^[48] Instead of relying solely on DFT for the structural optimization, we, thus, used DFT to construct a many-body interatomic potential, including two-body term (bond-stretching), three-body term (bond-bending), and four-body term (bond-torsion), and subsequently plugged it in Monte Carlo simulations easily yielding results for 10^4 atoms and more.^[48]

The curvature-induced excess energy, E_{excess} , represent the additional energy stored in a system as the C–C bonds are bent away from a flat graphene configuration in order to create a topologically closed fullerene surface. As the fullerene radius increases, the local configuration of atoms becomes flatter and better resembles planar arrangement of graphene, hence E_{excess} decreases (see Figure 9, only the MC data are shown). To quantify the excess energy, it was fitted with a power law,

$$E_{\text{excess}}^{\text{C}}(r) = \left(\frac{A}{r}\right)^{\beta} \quad (18)$$

The values of parameter β from DFT (1.43, only four data points fitted^[48]) and from MC (1.40) agree well, hence, verifying the multiscale/multimethod approach employed.^[48] Considering the excess surface energy alone is not sufficient anymore when more than one layer of atoms is present, as is the case in, for example, carbon onions. Then also induced dipole interactions (van der Waals interactions) have to be considered posing other modeling challenges.^[188,189]

The MC modeling revealed two crucial points.^[48] First, out of the three contributions to the excess energy, bond-stretching, bond-bending, and bond-torsion, the last is the largest. This is surprising, since it adds a very small value per a group of four atoms (defining the torsion), however, the

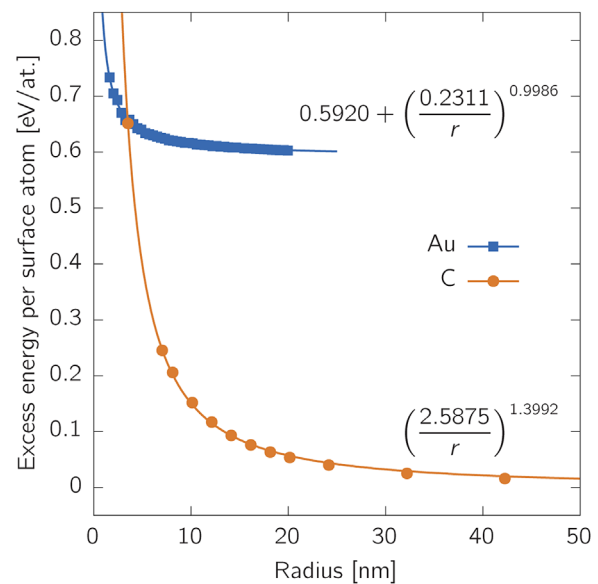


Fig. 9. Nanoparticles excess energy induced by curved topology of the hexagonal carbon cell (C fullerenes – orange, circles), and by existence of free surface (Au nanoparticles – blue squares).

torsion can not be satisfied by changing the radius of the fullerene, as is possible for bond-stretching and bending contributions. Consequently the torsion dominates over the latter two contributions. Second, the MC structurally relaxed large fullerenes revealed significant deviations from a spherical shape, in agreement with previous full “ab initio” calculations.^[190] Especially in the surroundings of each of the 12 pentagons, high local surface curvature was obtained, while areas between the pentagons, formed of hexagons, tend to flatten out (and, hence locally resemble graphene). Such geometry, however, is in contradiction with experimental observations using transmission electron microscope (TEM) suggesting a spherical shape. To solve this discrepancy, Bates and Scuseria^[191] suggested that defects, present experimentally either due to the fullerene growth process or the electron irradiation damage in TEM, restore the result in a spherical shape.

Gold nanoparticles serve as the second material system example. They are formed by cutting a defined shape from a bulk fcc–Au crystal. In our work,^[192] we considered spherical and cubic shapes, and cuboctahedrons. For the analysis below, we focus only the spherical nanoparticles, and use data calculated by MD with a potential shown to reproduce DFT-LDA surface and bulk properties.^[192] In contrast to the carbon fullerenes, gold nanoparticles are filled. A surface atom is defined as an atom with coordination lower than in the bulk, which for an fcc material is 12. The surface-induced excess energy, that is, in this case related to the presence of a free surface instead of a curved geometry, is defined as

$$E_{\text{excess}} = \frac{E_{\text{tot}} - NE_{\text{bulk}}(\text{Au})}{N_{\text{surf}}}, \quad (19)$$

where E_{tot} is the total energy of a nanoparticles consisting of N Au atoms. $E_{\text{bulk}}(\text{Au})$ is the total energy (per atom) of bulk fcc–Au, and N_{surf} is the number of surface atoms (i.e., those having coordination < 12). Again, it is possible to fit the obtained trend with a power law function

$$E_{\text{excess}}^{\text{Au}}(r) = \gamma + \left(\frac{A}{r}\right)^{\beta}. \quad (20)$$

Here, the constant γ relates to the surface energy. By fitting N_{surf} as a function of the nanosphere radius, r , $N_{\text{surf}} = 1.927r^2 \text{ \AA}^{-2}$, we obtained surface area corresponding to one surface atom

$$A_{\text{atom}} = \frac{4\pi r^2}{1.927r^2} \text{ \AA}^2 \approx 6.52 \text{ \AA}^2. \quad (21)$$

Therefore, the estimated surface energy of large spherical crystalline gold nanoparticles is $0.592 \text{ eV}/6.52 \text{ \AA}^2 \approx 1.44 \text{ J m}^{-2}$. This value agrees well with the surface energies of low-index facets of fcc–Au: $\gamma_{(100)} = 1.34$, $\gamma_{(110)} = 1.43$, and $\gamma_{(111)} = 1.26 \text{ J m}^{-2}$, hence justifying the chosen functional form of the fit.

It is striking to realise that the excess energy of both, shell-like carbon fullerenes as well as gold nanoparticles, follows the same dependence on the particle diameter, moreover considering the fact that the origin is different in each case. While for the fullerenes the excess stems from folding a planar graphene into a sphere (deforming bonds rather than breaking them), in the case of filled nanoparticles the excess is related to the presence of free surface, hence presence of broken bonds.

6. Conclusions and Outlook

The above collection of selected examples demonstrates the power of modern atomistic modeling based on quantum mechanical principles, as well as on classical interatomic potentials. This fast developing area has become an integral part of contemporary Materials Science. It provides a unique insight into the very fundamental principles of materials performance, complementing, and often extending the knowledge available from experiments. Although their interpretation must be done with care, acknowledging the reality, and checking the calculated results against experiments, in many cases, the obtained results do not provide only qualitative, but more and more often also quantitative description of wide range of physical and chemical phenomena and are helpful for further developments of today’s technology and materials processing.

The near future DFT applications for investigations of material properties and for prediction of novel materials with tailored technological specifications may be foreseen, and has already started, in four basic directions (for each area we provide several references, which coin the path):

- 1) finite temperature effects,^[37,38,125,127,129,131–134,160]
- 2) extended defects (grain boundaries, stacking faults, dislocations, etc.),^[8,98,193–209]
- 3) materials of relevance for real applications (complex compositions, realistic conditions, etc.),^[31,63,68,159,160,176,179,210–215] and
- 4) high-throughput search for novel materials^[13,215–221] using databases such as flowlib.org,^[222] oqmd.org,^[223] nomad-repository.eu, aiida.net,^[224] or materialsproject.org^[225] which can be efficiently accessed by their own online interfaces or Python libraries, for example, [pymatgen](http://pymatgen.org).^[226]

For efficient implementation of points 2) and 3) it is envisioned that a multimethod/multiscale approaches,^[9,48,162,163,169,227–231] combining DFT, atomistic, and continuum modeling will be essential. Our group at the Montanuniversität Leoben together with its collaborating partners has been devoted to contribute substantially to this challenging and exciting research.

Article first published online: January 10, 2017

Manuscript Revised: November 24, 2016

Manuscript Received: September 30, 2016

- [1] R. LeSar, *Introduction to Computational Materials Science: Fundamentals to Applications*, Cambridge University Press, Cambridge, UK **2013**.
- [2] D. Alfè, G. D. Price, M. J. Gillan, *Phys. Rev. B* **2002**, *65*, 165118. doi:10.1103/PhysRevB.65.165118
- [3] X. Huang, G. J. Ackland, K. M. Rabe, *Nat. Mater.* **2003**, *2*, 307. doi:10.1038/nmat884
- [4] R. F. Zhang, S. Veprek, *Acta Mater.* **2009**, *57*, 2259. doi:10.1016/j.actamat.2009.01.028
- [5] C. Höglund, B. Alling, J. Birch, M. Beckers, P. O. A. Persson, C. Baetz, Z. Czigány, J. Jensen, L. Hultman, *Phys. Rev. B* **2010**, *81*, 224101. doi:10.1103/PhysRevB.81.224101
- [6] D. Holec, R. Rachbauer, L. Chen, L. Wang, D. Luef, P. H. Mayrhofer, *Surf. Coat. Technol.* **2011**, *206*, 1698. doi:10.1016/j.surfcoat.2011.09.019
- [7] P. Erdely, R. Werner, E. Schwaighofer, H. Clemens, S. Mayer, *Intermetallics* **2015**, *57*, 174. doi:10.1016/j.intermet.2014.09.011
- [8] M. Friák, D. Tytko, D. Holec, P.-P. Choi, P. Eisenlohr, D. Raabe, J. Neugebauer, *New J. Phys.* **2015**, *17*, 093004. doi:10.1088/1367-2630/17/9/093004
- [9] M. Bartosik, M. Todt, D. Holec, J. Todt, L. Zhou, H. Riedl, H. J. Böhm, F. G. Rammerstorfer, P. H. Mayrhofer, *Appl. Phys. Lett.* **2015**, *107*, 071602. doi:10.1063/1.4928911
- [10] D. M. Clatterbuck, C. R. Krenn, M. L. Cohen, J. W. Morris, *Phys. Rev. Lett.* **2003**, *91*, 135501. doi:10.1103/PhysRevLett.91.135501
- [11] R. F. Zhang, A. S. Argon, S. Veprek, *Phys. Rev. B* **2009**, *79*, 245426. doi:10.1103/PhysRevB.79.245426
- [12] J. Pi, Y. Kong, L. Chen, Y. Du, *Appl. Surf. Sci.* **2016**, *378*, 293. doi:10.1016/j.apsusc.2016.04.002
- [13] S. Curtarolo, G. L. W. Hart, M. B. Nardelli, N. Mingo, S. Sanvito, O. Levy, *Nat. Mater.* **2013**, *12*, 191. doi:10.1038/nmat3568
- [14] P. Hohenberg, W. Kohn, *Phys. Rev.* **1964**, *136*, B864.
- [15] W. Kohn, L. J. Sham, *Phys. Rev.* **1965**, *140*, A1133.
- [16] J. G. Lee, *Computational Materials Science: An Introduction*, CRC Press, Boca Raton, FL **2011**.
- [17] G. Lu, E. B. Tadmor, E. Kaxiras, *Phys. Rev. B* **2006**, *73*, 024108. doi:10.1103/PhysRevB.73.024108
- [18] G. Kresse, J. Furthmüller, *Phys. Rev. B* **1996**, *54*, 11169. doi:10.1103/PhysRevB.54.11169
- [19] G. Kresse, J. Furthmüller, *Comput. Mater. Sci.* **1996**, *6*, 15. doi:10.1016/0927-0256(96)00008-0
- [20] J. Hafner, *Comput. Chem.* **2008**, *29*, 2044. doi:10.1002/jcc.21057
- [21] P. Blaha, K. Schwarz, G. Madsen, D. Kvasnicka, J. Luitz, *WIEN2k, An Augmented Plane Wave + Local Orbitals Program for Calculating Crystal Properties*, Karlheinz Schwarz, Techn. Universität Wien, Austria **2001**.
- [22] T. Ozaki, *Phys. Rev. B* **2003** *67*. doi:10.1103/PhysRevB.67.155108
- [23] T. Ozaki, H. Kino, *Phys. Rev. B* **2005** *72*. doi:10.1103/PhysRevB.72.045121
- [24] Y. Wang, J. P. Perdew, *Phys. Rev. B* **1991**, *44*, 13298. doi:10.1103/PhysRevB.44.13298
- [25] J. P. Perdew, K. Burke, M. Ernzerhof, *Phys. Rev. Lett.* **1996**, *77*, 3865. doi:10.1103/PhysRevLett.77.3865
- [26] H. J. Monkhorst, J. D. Pack, *Phys. Rev. B* **1976**, *13*, 5188. doi:10.1103/PhysRevB.13.5188
- [27] S.-H. Wei, L. G. Ferreira, J. Bernard, A. Zunger, *Phys. Rev. B: Condens. Matter* **1990**, *42*, 9622. doi:10.1103/PhysRevB.42.9622
- [28] J. V. Pezold, A. Dick, M. Friák, J. Neugebauer, *Phys. Rev. B* **2010**, *81*, 094203. doi:10.1103/PhysRevB.81.094203
- [29] S. Müller, *J. Phys. Condens. Matter* **2003**, *15*, R1429. doi:10.1088/0953-8984/15/34/201
- [30] A. van de Walle, *CALPHAD* **2009**, *33*, 266. doi:10.1016/j.calphad.2008.12.005
- [31] D. Holec, L. Zhou, R. Rachbauer, P. H. Mayrhofer, in *Density Functional Theory: Principles, Applications and Analysis* (Eds: J. M. Pelletier, J. Morin), Nova Publishers, New York **2013**, p. 259.
- [32] C. Jiang, B. P. Uberuaga, *Phys. Rev. Lett.* **2016**, *116*, 105501. doi:10.1103/PhysRevLett.116.105501
- [33] A. van de Walle, P. Tiwary, M. de Jong, D. L. Olmsted, M. Asta, A. Dick, D. Shin, Y. Wang, L.-Q. Chen, Z.-K. Liu, *CALPHAD* **2013**, *42*, 13. doi:10.1016/j.calphad.2013.06.006
- [34] F. Tasnádi, M. Odén, I. A. Abrikosov, *Phys. Rev. B* **2012**, *85*, 144112. doi:10.1103/PhysRevB.85.144112
- [35] F. Tasnádi, F. Wang, M. Odén, I. A. Abrikosov, *Comput. Mater. Sci.* **2015**, *103*, 194. doi:10.1016/j.commatsci.2015.03.030
- [36] B. Alling, T. Marten, I. A. Abrikosov, *Phys. Rev. B* **2010**, *82*, 184430. doi:10.1103/PhysRevB.82.184430
- [37] L. Zhou, F. Körmann, D. Holec, M. Bartosik, B. Grabowski, J. Neugebauer, P. H. Mayrhofer, *Phys. Rev. B* **2014**, *90*, 184102. doi:10.1103/PhysRevB.90.184102
- [38] N. Shulumba, B. Alling, O. Hellman, E. Mozafari, P. Steneteg, M. Odén, I. A. Abrikosov, *Phys. Rev. B* **2014**, *89*, 174108. doi:10.1103/PhysRevB.89.174108
- [39] C. Hébert, *Micron* **2007**, *38*, 12. doi:10.1016/j.micron.2006.03.010
- [40] H. Titrian, U. Aydin, M. Friák, D. Ma, D. Raabe, J. Neugebauer, *Mater. Res. Soc. Symp. Proc.* **2013**, *1524*, 152.
- [41] M. Friák, W. A. Counts, D. Ma, B. Sander, D. Holec, D. Raabe, J. Neugebauer, *Materials* **2012**, *5*, 1853. doi:10.3390/ma5101853
- [42] L.-F. Zhu, M. Friák, L. Lymperakis, H. Titrian, U. Aydin, A. M. Janus, H.-O. Fabritius, A. Ziegler, S. Nikolov, P. Hemzalová, D. Raabe, J. Neugebauer, *J. Mech. Behav. Biomed. Mater.* **2013**, *20*, 296. doi:10.1016/j.jmbbm.2013.01.030
- [43] A. Togo, I. Tanaka, *Scr. Mater.* **2015**, *108*, 1. doi:10.1016/j.scripamat.2015.07.021

- [44] A. Togo, L. Chaput, I. Tanaka, G. Hug, *Phys. Rev. B* **2011**, *81*(17), 174301.
- [45] F. Körmann, A. Dick, B. Grabowski, T. Hickel, J. Neugebauer, *Phys. Rev. B* **2012**, *85*, 125104. doi:10.1103/PhysRevB.85.125104
- [46] K. Momma, F. Izumi, *J. Appl. Crystallogr.* **2011**, *44*, 1272. doi:10.1107/S0021889811038970
- [47] K. Binder, *Rep. Prog. Phys.* **1999**, *60*, 487. doi:10.1088/0034-4885/60/5/001
- [48] D. Holec, M. A. Hartmann, F. D. Fischer, F. G. Rammerstorfer, P. H. Mayrhofer, O. Paris, *Phys. Rev. B* **2010**, *81*, 235403. doi:10.1103/PhysRevB.81.235403
- [49] M. A. Hartmann, M. Todt, F. G. Rammerstorfer, in *Structure and Multiscale Mechanics of Carbon Nanomaterials*, Vol. 563 (Ed: O. Paris), CISM, Springer, Vienna **2016**. doi:10.1007/978-3-7091-1887-0_6
- [50] S. Plimpton, *J. Comput. Phys.* **1995**, *117*, 1. doi:10.1006/jcph.1995.1039
- [51] G. Grochola, S. P. Russo, I. K. Snook, *J. Chem. Phys.* **2005**, *123*, 204719. doi:10.1063/1.2124667
- [52] L. Rogström, M. P. Johansson, N. Ghafoor, L. Hultman, M. Odén, *J. Vac. Sci. Technol. A* **2012**, *30*, 031504. doi:10.1116/1.3698592
- [53] P. Mayrhofer, D. Sonnleitner, M. Bartosik, D. Holec, *Surf. Coat. Technol.* **2014**, *244*, 52. doi:10.1016/j.surfcoat.2014.01.049
- [54] R. Franz, M. Lechthaler, C. Polzer, C. Mitterer, *Surf. Coat. Technol.* **2012**, *206*, 2337. doi:10.1016/j.surfcoat.2011.10.023
- [55] G. M. Matenoglou, C. E. Lekka, L. E. Koutsokeras, G. Karras, C. Kosmidis, G. A. Evangelakis, P. Patsalas, *J. Appl. Phys.* **2009**, *105*, 103714. doi:10.1063/1.3131824
- [56] D. Holec, R. Franz, P. H. Mayrhofer, C. Mitterer, *J. Phys. D Appl. Phys.* **2010**, *43*, 145403.
- [57] R. Rachbauer, D. Holec, P. H. Mayrhofer, *Appl. Phys. Lett.* **2010**, *97*, 151901. doi:10.1063/1.3495783
- [58] P. H. Mayrhofer, R. Rachbauer, D. Holec, *Scr. Mater.* **2010**, *63*, 807. doi:10.1016/j.scriptamat.2010.06.020
- [59] L. E. Koutsokeras, G. Abadias, P. Patsalas, *J. Appl. Phys.* **2011**, *110*, 043535. doi:10.1063/1.3622585
- [60] I. A. Abrikosov, A. Knutsson, B. Alling, F. Tasnádi, H. Lind, L. Hultman, M. Odén, *Materials* **2011**, *4*, 1599. doi:10.3390/ma4091599
- [61] H. Riedl, D. Holec, R. Rachbauer, P. Polcik, R. Hollerweger, J. Paulitsch, P. H. Mayrhofer, *Surf. Coat. Technol.* **2013**, *235*, 174. doi:10.1016/j.surfcoat.2013.07.030
- [62] P. H. Mayrhofer, R. Rachbauer, D. Holec, F. Rovere, J. M. Schneider, in *Comprehensive Materials Processing* (Eds: S. Hashmi, G. F. Batalha, C. J. V. Tyne, B. Yilbas), Elsevier, Oxford **2014**, p. 355. doi:10.1016/B978-0-08-096532-1.00423-4
- [63] D. Music, R. W. Geyer, J. M. Schneider, *Surf. Coat. Technol.* **2016**, *286*, 178. doi:10.1016/j.surfcoat.2015.12.021
- [64] S. S. Kim, T. H. Sanders Jr, *J. Am. Ceram. Soc.* **2001**, *84*, 1881. doi:10.1111/j.1151-2916.2001.tb00930.x
- [65] K. Bobzin, N. Bagcivan, A. Reinholdt, M. Ewering, *Surf. Coat. Technol.* **2010**, *205*, 1444. doi:10.1016/j.surfcoat.2010.07.040
- [66] B. Alling, A. Khatibi, S. I. Simak, P. Eklund, L. Hultman, *J. Vac. Sci. Technol. A* **2013**, *31*, 030602. doi:10.1116/1.4795392
- [67] F. Nahif, D. Music, S. Mráz, M. to Baben, J. M. Schneider, *J. Phys. Condens. Matter* **2013**, *25*, 125502. doi:10.1088/0953-8984/25/12/125502
- [68] C. M. Koller, N. Koutná, J. Ramm, S. Kolozsvári, J. Paulitsch, D. Holec, P. H. Mayrhofer, *AIP Adv.* **2016**, *6*, 025002. doi:10.1063/1.4941573
- [69] V. Edlmayr, M. Moser, C. Walter, C. Mitterer, *Surf. Coat. Technol.* **2010**, *204*, 1576. doi:10.1016/j.surfcoat.2009.10.002
- [70] C. Mitterer, in *Comprehensive Hard Materials* (Ed: V. K. Sarin), Elsevier, Oxford **2014**, p. 449. doi:10.1016/B978-0-08-096527-7.00035-0
- [71] D. Music, F. Nahif, K. Sarakinos, N. Friederichsen, J. M. Schneider, *Appl. Phys. Lett.* **2011**, *98*, 111908. doi:10.1063/1.3570650
- [72] J. Houska, *Surf. Coat. Technol.* **2013**, *235*, 333. doi:10.1016/j.surfcoat.2013.07.062
- [73] H. Euchner, P. H. Mayrhofer, *Surf. Coat. Technol.* **2015**, *275*, 214. doi:10.1016/j.surfcoat.2015.05.017
- [74] M. Hans, M. to Baben, D. Music, J. Ebenhöch, D. Primetzhofer, D. Kurapov, M. Arndt, H. Rudigier, J. M. Schneider, *J. Appl. Phys.* **2014**, *116*, 093515. doi:10.1063/1.4894776
- [75] N. Schalk, J. F. T. Simonet Fotso, D. Holec, A. Fian, G. Jakopic, V. L. Terziyska, R. Daniel, C. Mitterer, *J. Phys. D Appl. Phys.* **2016**, *49*, 025307. doi:10.1088/0022-3727/49/2/025307
- [76] N. Schalk, J. F. T. Simonet Fotso, D. Holec, G. Jakopic, A. Fian, V. L. Terziyska, R. Daniel, C. Mitterer, *Acta Mater.* **2016**, *119*, 26. doi:10.1016/j.actamat.2016.08.007
- [77] T. Klein, B. Rashkova, D. Holec, H. Clemens, S. Mayer, *Acta Mater.* **2016**, *110*, 236. doi:10.1016/j.actamat.2016.03.050
- [78] G. Ressel, D. Holec, A. Fian, F. Mendez-Martin, H. Leitner, *Appl. Phys. A: Mater. Sci. Process.* **2014**, *115*(3), 851. doi:10.1007/s00339-013-7877-y
- [79] A. Dick, B. Grabowski, T. Hickel, F. Liot, D. Holec, A. Schlieter, U. Ku, J. Eckert, Z. Ebrahimi, H. Emmerich, J. Neugebauer, L.-F. Zhu, M. Friák, U. Kühn, *Acta Mater.* **2012**, *60*, 1594. doi:10.1016/j.actamat.2011.11.046
- [80] D. Lang, C. Pöhl, D. Holec, J. Schatte, E. Povoden-Karadeniz, W. Knabl, H. Clemens, S. Primig, *J. Alloys Compd.* **2016**, *654*, 445. doi:10.1016/j.jallcom.2015.09.126
- [81] K. P. Shaha, H. Rueß, S. Rotert, M. to Baben, D. Music, J. M. Schneider, *Appl. Phys. Lett.* **2013**, *103*, 221905. doi:10.1063/1.4833835

- [82] H. Euchner, P. H. Mayrhofer, H. Riedl, F. F. Klimashin, A. Limbeck, P. Polcik, S. Kolozsvari, *Acta Mater.* **2015**, *101*, 55. doi:10.1016/j.actamat.2015.08.048
- [83] H. Euchner, P. H. Mayrhofer, *Thin Solid Films* **2015**, *583*, 46. doi:10.1016/j.tsf.2015.03.035
- [84] P. Ondračka, D. Holec, D. Nečas, L. Zajčková, *J. Phys. D Appl. Phys.* **2016**, *49*, 395301. doi:10.1088/0022-3727/49/39/395301
- [85] D. Holec, R. Rachbauer, D. Kiener, P. D. Cherns, P. M. F. J. Costa, C. McAleese, P. H. Mayrhofer, C. J. Humphreys, *Phys. Rev. B* **2011**, *83*, 165122. doi:10.1103/PhysRevB.83.165122
- [86] P. H. Mayrhofer, D. Music, J. M. Schneider, *J. Appl. Phys.* **2006**, *100*, 094906. doi:10.1063/1.2360778
- [87] Z. Zhang, R. Daniel, C. Mitterer, *J. Appl. Phys.* **2011**, *110*, 043524. doi:10.1063/1.3624772
- [88] Z. Zhang, H. Li, R. Daniel, C. Mitterer, G. Dehm, *Phys. Rev. B* **2013**, *87*, 014104. doi:10.1103/PhysRevB.87.014104
- [89] J. F. Nye, *Physical Properties of Crystals*, Clarendon Press, Oxford **1957**.
- [90] R. Yu, J. Zhu, H. Ye, *Comput. Phys. Commun.* **2010**, *181*, 671. doi:10.1016/j.cpc.2009.11.017
- [91] M. A. Caro, S. Schulz, E. P. O'Reilly, *J. Phys. Condens. Matter* **2013**, *25*, 025803. doi:10.1088/0953-8984/25/2/025803
- [92] J. Zhao, J. M. Winey, Y. M. Gupta, *Phys. Rev. B* **2007**, *75*, 94105. doi:10.1103/PhysRevB.75.094105
- [93] M. Lopuszynski, J. A. Majewski, *Phys. Rev. B* **2007**, *76*, 045202. doi:10.1103/PhysRevB.76.045202
- [94] D. Holec, M. Friák, J. Neugebauer, P. H. Mayrhofer, *Phys. Rev. B* **2012**, *85*, 064101. doi:10.1103/PhysRevB.85.064101
- [95] R. Golesorkhtabar, P. Pavone, J. Spitaler, P. Puschnig, C. Draxl, *Comput. Phys. Commun.* **2013**, *184*, 1861. doi:10.1016/j.cpc.2013.03.010
- [96] M. Petrov, L. Lymperakis, J. Neugebauer, R. Stefaniuk, P. Dłuzewski, in *Proceedings of the Computer Methods in Mechanics*, June 19-22 2007, Poland. **2007**.
- [97] H. H. Pham, M. E. Williams, P. Mahaffey, M. Radovic, R. Arroyave, T. Cagin, *Phys. Rev. B* **2011**, *84*, 064101. doi:10.1103/PhysRevB.84.064101
- [98] L. Liu, X. Wu, R. Wang, W. Li, Q. Liu, *Comput. Mater. Sci.* **2015**, *103*, 116. doi:10.1016/j.commatsci.2015.03.024
- [99] N. Shulumba, O. Hellman, L. Rogström, Z. Raza, F. Tasnádi, I. A. Abrikosov, M. Odén, *Appl. Phys. Lett.* **2015**, *107*, 231901. doi:10.1063/1.4936896
- [100] L. Zhou, D. Holec, P. H. Mayrhofer, *J. Appl. Phys.* **2013**, *113*, 043511. doi:10.1063/1.4789378
- [101] F. Tasnádi, I. A. Abrikosov, L. Rogström, J. Almer, M. P. Johansson, M. Odén, *Appl. Phys. Lett.* **2010**, *97*, 231902. doi:10.1063/1.3524502
- [102] S. Zhang, W. Y. Fu, D. Holec, C. J. Humphreys, M. A. Moram, *J. Appl. Phys.* **2013**, *114*, 243516. doi:10.1063/1.4848036
- [103] D. Holec, F. Tasnádi, P. Wagner, M. Friák, J. Neugebauer, P. H. Mayrhofer, J. Keckes, *Phys. Rev. B* **2014**, *90*, 184106. doi:10.1103/PhysRevB.90.184106
- [104] L. Zhou, F. F. Klimashin, D. Holec, P. H. Mayrhofer, *Scr. Mater.* **2016**, *123*, 34. doi:10.1016/j.scriptamat.2016.05.036
- [105] M. Friák, T. Hickel, F. Körmann, A. Udyansky, A. Dick, J. von Pezold, D. Ma, O. Kim, W. Counts, M. Šob, T. Gebhardt, D. Music, J. Schneider, D. Raabe, J. Neugebauer, *Steel Res. Int.* **2011**, *82*, 86. doi:10.1002/srin.201000264
- [106] R. Hill, *Proc. Phys. Soc. A* **1952**, *65*, 349. doi:10.1088/0370-1298/65/5/307
- [107] S. F. Pugh, *Philos. Mag.* **1954**, *45*, 823. doi:10.1080/14786440808520496
- [108] K. Kutschej, P. H. Mayrhofer, M. Kathrein, P. Polcik, R. Tessadri, C. Mitterer, *Surf. Coat. Technol.* **2005**, *200*, 2358. doi:10.1016/j.surfcoat.2004.12.008
- [109] H. Ljungcrantz, M. Odén, L. Hultman, J. E. Greene, J.-E. Sundgren, *J. Appl. Phys.* **1996**, *80*, 6725. doi:10.1063/1.363799
- [110] F. F. Klimashin, H. Riedl, D. Primetzhofer, J. Paulitsch, P. H. Mayrhofer, *J. Appl. Phys.* **2015**, *118*, 025305. doi:10.1063/1.4926734
- [111] M. Born, K. Huang, *Dynamical Theory of Crystal Lattices*, Clarendon Press, Oxford and New York **1954**.
- [112] F. Mouhat, F.-X. Coudert, *Phys. Rev. B* **2014**, *90*, 224104. doi:10.1103/PhysRevB.90.224104
- [113] D. Holec, D. Legut, L. Isaeva, P. Souvatzis, H. Clemens, S. Mayer, *Intermetallics* **2015**, *61*, 85. doi:10.1016/j.intermet.2015.03.001
- [114] D. Holec, R. K. Reddy, T. Klein, H. Clemens, *J. Appl. Phys.* **2016**, *119*, 205104. doi:10.1063/1.4951009
- [115] T. Cheng, M. Willis, I. Jones, *Intermetallics* **1999**, *7*, 89. doi:10.1016/S0966-9795(98)00016-8
- [116] S. Mayer, C. Sailer, H. Nakashima, T. Schmoelzer, T. Lippmann, P. Staron, K.-D. Liss, H. Clemens, M. Takeyama, in *MRS Proceedings Vol. 1295*, Cambridge University Press **2011**, p. 113. doi:10.1557/opl.2011.31
- [117] J. Pokluda, M. Černý, M. Šob, Y. Umeno, *Prog. Mater. Sci.* **2015**, *73*, 127. doi:10.1016/j.pmatsci.2015.04.001
- [118] M. Šob, M. Friák, D. Legut, J. Fiala, V. Vitek, *Mat. Sci. Eng. A* **2004**, *387-389*, 148.
- [119] S. Ogata, Y. Umeno, M. Kohyama, *Modell. Simul. Mater. Sci. Eng.* **2009**, *17*, 013001. doi:10.1088/0965-0393/17/1/013001
- [120] G. Grimvall, B. Magyari-Köpe, V. Ozolinš, K. A. Persson, *Rev. Mod. Phys.* **2012**, *84*, 945. doi:10.1103/RevModPhys.84.945
- [121] S. M.-M. Dubois, G.-M. Rignanese, T. Pardoën, J.-C. Charlier, *Phys. Rev. B* **2006**, *74*, 235203. doi:10.1103/PhysRevB.74.235203
- [122] P. Řehák, M. Černý, M. Šob, *Modell. Simul. Mater. Sci. Eng.* **2015**, *23*, 055010. doi:10.1088/0965-0393/23/5/055010

- [123] M. Palumbo, S. G. Fries, A. D. Corso, F. Körmann, T. Hickel, J. Neugebauer, *J. Phys. Condens. Matter* **2014**, *26*, 335401. doi:10.1088/0953-8984/26/33/335401
- [124] S. Baroni, S. de Gironcoli, A. D. Corso, P. Giannozzi, *Rev. Mod. Phys.* **2001**, *73*, 515. doi:10.1103/RevModPhys.73.515
- [125] B. Grabowski, L. Ismer, T. Hickel, J. Neugebauer, *Phys. Rev. B* **2009**, *79*, 134106. doi:10.1103/PhysRevB.79.134106
- [126] A. Glensk, B. Grabowski, T. Hickel, J. Neugebauer, *Phys. Rev. Lett.* **2015**, *114*, 195901. doi:10.1103/PhysRevLett.114.195901
- [127] A. I. Duff, T. Davey, D. Korbmacher, A. Glensk, B. Grabowski, J. Neugebauer, M. W. Finnis, *Phys. Rev. B* **2015**, *91*, 214311. doi:10.1103/PhysRevB.91.214311
- [128] I. A. Abrikosov, A. V. Ponomareva, P. Steneteg, S. A. Barannikova, B. Alling, *Curr. Opin. Solid State Mater. Sci.* **2016**, *20*, 85. doi:10.1016/j.cossms.2015.07.003
- [129] F. Körmann, T. Hickel, J. Neugebauer, *Curr. Opin. Solid State Mater. Sci.* **2016**, *20*, 77. doi:10.1016/j.cossms.2015.06.001
- [130] F. Körmann, A. Dick, B. Grabowski, B. Hallstedt, T. Hickel, J. Neugebauer, *Phys. Rev. B* **2008**, *78*, 033102. doi:10.1103/PhysRevB.78.033102
- [131] F. Körmann, A. Dick, T. Hickel, J. Neugebauer, *Phys. Rev. B* **2010**, *81*, 134425. doi:10.1103/PhysRevB.81.134425
- [132] F. Körmann, A. Dick, T. Hickel, J. Neugebauer, *Phys. Rev. B* **2011**, *83*, 165114. doi:10.1103/PhysRevB.83.165114
- [133] F. Körmann, B. Grabowski, P. Söderlind, M. Palumbo, S. G. Fries, T. Hickel, J. Neugebauer, *J. Phys.: Condens. Matter* **2013**, *25*, 425401. doi:10.1088/0953-8984/25/42/425401.
- [134] F. Körmann, B. Grabowski, B. Dutta, T. Hickel, L. Mauger, B. Fultz, J. Neugebauer, *Phys. Rev. Lett.* **2014**, *113*, 165503. doi:10.1103/PhysRevLett.113.165503
- [135] F. Körmann, P.-W. Ma, S. L. Dudarev, J. Neugebauer, *J. Phys.: Condens. Matter* **2016**, *28*, 076002. doi:10.1088/0953-8984/28/7/076002
- [136] B. Alling, F. Körmann, B. Grabowski, A. Glensk, I. Abrikosov, J. Neugebauer, *Phys. Rev. B* **2016**, *93*, 224411. doi:10.1103/PhysRevB.93.224411
- [137] B. Hallstedt, D. Djurovic, J. von Appen, R. Dronskowski, A. Dick, F. Körmann, T. Hickel, J. Neugebauer, *CALPHAD* **2010**, *34*, 129. doi:https://doi.org/10.1016/j.calphad.2010.01.004
- [138] A. Dick, F. Körmann, T. Hickel, J. Neugebauer, *Phys. Rev. B* **2011**, *84*, 125101. doi:10.1103/PhysRevB.84.125101
- [139] A. Löffler, A. Zendegani, J. Gröbner, M. Hampl, R. Schmid-Fetzer, H. Engelhardt, M. Rettenmayr, F. Körmann, T. Hickel, J. Neugebauer, *J. Phase Equilib. Diffus.* **2016**, *37*, 119. doi:10.1007/s11669-015-0426-y
- [140] F. Körmann, A. V. Ruban, M. H. Sluiter, *Mater. Res. Lett.* **2017**, *5*(1), 35. doi:10.1080/21663831.2016.1198837
- [141] F. Körmann, M. H. Sluiter, *Entropy* **2016**, *18*, 403. doi:10.3390/e18080403
- [142] F. Körmann, A. A. H. Breidi, S. L. Dudarev, N. Dupin, G. Ghosh, T. Hickel, P. Korzhavyi, J. A. Muñoz, I. Ohnuma, *Phys. Status Solidi B* **2014**, *251*, 53. doi:10.1002/pssb.201350136
- [143] B. Grabowski, T. Hickel, J. Neugebauer, *Phys. Rev. B* **2007**, *76*, 024309. doi:10.1103/PhysRevB.76.024309
- [144] T. Hickel, B. Grabowski, F. Körmann, J. Neugebauer, *J. Phys. Condens. Matter* **2012**, *24*, 053202. doi:10.1088/0953-8984/24/5/053202
- [145] A. V. Ruban, I. A. Abrikosov, *Rep. Prog. Phys.* **2008**, *71*, 046501. doi:10.1088/0034-4885/71/4/046501
- [146] P. Souvatzis, O. Eriksson, M. I. Katsnelson, S. P. Rudin, *Phys. Rev. Lett.* **2008**, *100*, 095901.
- [147] P. Souvatzis, O. Eriksson, M. I. Katsnelson, S. P. Rudin, *Comput. Mater. Sci.* **2009**, *44*, 888. doi:10.1016/j.commatsci.2008.06.016
- [148] P. Souvatzis, D. Legut, O. Eriksson, M. I. Katsnelson, *Phys. Rev. B* **2010**, *81*, 092201. doi:10.1103/PhysRevB.81.092201
- [149] V. Ozolins, *Phys. Rev. Lett.* **2009**, *102*, 065702. doi:10.1103/PhysRevLett.102.065702
- [150] N. Antolin, O. D. Restrepo, W. Windl, *Phys. Rev. B* **2012**, *86*, 054119. doi:10.1103/PhysRevB.86.054119
- [151] I. Errea, M. Calandra, F. Mauri, *Phys. Rev. Lett.* **2013**, *111*, 177002. doi:10.1103/PhysRevLett.111.177002
- [152] F. Rovere, D. Music, S. Ershov, M. to Baben, H.-G. Fuss, P. H. Mayrhofer, J. M. Schneider, *J. Phys. D Appl. Phys.* **2010**, *43*, 035302. doi:10.1088/0022-3727/43/3/035302
- [153] D. Music, P. Bliem, M. Hans, *Solid State Commun.* **2015**, *212*, 5. doi:10.1016/j.ssc.2015.03.020
- [154] D. Holec, T. Schmoelzer, P. Staron, D. Legut, A. Stark, T. Lippmann, M. Blankenburg, H. Clemens, S. Mayer, Thermal expansion and heat capacity of α - and γ -phases in an intermetallic γ -TiAl based alloy, in preparation.
- [155] J. P. Perdew, K. Schmidt, *AIP Conf. Proc.* **2001**, *577*, 1. doi:10.1063/1.1390175
- [156] P. Haas, F. Tran, P. Blaha, *Phys. Rev. B* **2009**, *79*, 085104. doi:10.1103/PhysRevB.79.085104
- [157] B. Grabowski, S. Wippermann, A. Glensk, T. Hickel, J. Neugebauer, *Phys. Rev. B* **2015**, *91*, 201103. doi:10.1103/PhysRevB.91.201103
- [158] H. Sawada, K. Kawakami, F. Körmann, B. Grabowski, T. Hickel, J. Neugebauer, *Acta Mater.* **2016**, *102*, 241. doi:10.1016/j.actamat.2015.09.010
- [159] F. Körmann, D. Ma, D. D. Belyea, M. S. Lucas, C. W. Miller, B. Grabowski, M. H. Sluiter, *Appl. Phys. Lett.* **2015**, *107*, 142404. doi:10.1063/1.4932571
- [160] D. Ma, B. Grabowski, F. Körmann, J. Neugebauer, D. Raabe, *Acta Mater.* **2015**, *100*, 90. doi:10.1016/j.actamat.2015.08.050

- [161] J. Havránková, J. Vřešťál, L. G. Wang, M. Šob, *Phys. Rev. B* **2001**, *63*, 174104. doi:10.1103/PhysRevB.63.174104
- [162] J. Houserová, J. Vřešťál, M. Friák, M. Šob, *CALPHAD* **2002**, *26*, 513. doi:10.1016/S0364-5916(02)80004-9
- [163] J. Houserová, M. Friák, M. Šob, J. Vřešťál, *Comput. Mater. Sci.* **2002**, *25*, 562. doi:10.1016/S0927-0256(02)00335-X
- [164] B. Sundman, H. L. Lukas, S. G. Fries, *Computational thermodynamics: The CALPHAD method*, Cambridge University Press, New York **2007**.
- [165] Z.-K. Liu, *J. Phase Equilib. Diffus.* **2009**, *30*, 517. doi:10.1007/s11669-009-9570-6
- [166] Y. Wang, S. Shang, L.-Q. Chen, Z.-K. Liu, *JOM* **2013**, *65*, 1533. doi:10.1007/s11837-013-0751-8
- [167] J.-O. Andersson, T. Helander, L. Höglund, P. Shi, B. Sundman, *CALPHAD* **2002**, *26*, 273. doi:10.1016/S0364-5916(02)00037-8
- [168] E. Kozeschnik, *Modeling Solid-State Precipitation*, Momentum Press, New York **2012**. doi:10.5643/9781606500644
- [169] M. Šob, A. Kroupa, J. Vřešťál, *Solid State Phenom.* **2009**, *150*, 1. doi:10.4028/www.scientific.net/SSP.150.1
- [170] J. Rogal, S. V. Divinski, M. W. Finnis, A. Glensk, J. Neugebauer, J. H. Perepezko, S. Schuwalow, M. H. F. Sluiter, B. Sundman, *Phys. Status Solidi* **2014**, *251*, 97.
- [171] T. Hammerschmidt, I. A. Abrikosov, D. Alfè, S. G. Fries, L. Höglund, M. Jacobs, J. Koßmann, X.-G. Lu, G. Paul, *Phys. Status Solidi* **2014**, *251*, 81.
- [172] C. A. Becker, J. Agren, M. Baricco, Q. Chen, S. A. Decterov, U. R. Kattner, J. H. Perepezko, G. R. Pottlacher, M. Selleby, *Phys. Status Solidi* **2014**, *251*, 33.
- [173] M. Palumbo, B. Burton, A. Costa e Silva, B. Fultz, B. Grabowski, G. Grimvall, B. Hallstedt, O. Hellman, B. Lindahl, A. Schneider, *Others, Phys. Status Solidi* **2014**, *251*, 14.
- [174] F. Appel, H. Clemens, F. D. Fischer, *Prog. Mater. Sci.* **2016**, *81*, 55. doi:10.1016/j.pmatsci.2016.01.001
- [175] S. Mayer, P. Erdely, F. D. Fischer, D. Holec, M. Kastenhuber, T. Klein, H. Clemens, Intermetallic titanium aluminides - from fundamental research to application, under review in AEM.
- [176] D. Holec, J. Paulitsch, P. H. Mayrhofer, *Solid State Phenom.* **2016**, *258*, 373. doi:10.4028/www.scientific.net/SSP.258.373
- [177] J. Paulitsch, M. Schenkel, A. Schintlmeister, H. Hutter, P. H. Mayrhofer, *Thin Solid Films* **2010**, *518*, 5553. doi:10.1016/j.tsf.2010.05.061
- [178] O. Jantschner, S. K. Field, D. Music, V. L. Terziyska, J. M. Schneider, F. Munnik, K. Zorn, C. Mitterer, *Tribol. Int.* **2014**, *77*, 15. doi:10.1016/j.triboint.2014.04.006
- [179] O. Jantschner, S. K. Field, D. Holec, A. Fian, D. Music, J. M. Schneider, K. Zorn, C. Mitterer, *Acta Mater.* **2015**, *82*, 437. doi:10.1016/j.actamat.2014.09.030
- [180] T.-B. Ma, Y.-Z. Hu, L. Xu, L.-F. Wang, H. Wang, *Chem. Phys. Lett.* **2011**, *514*, 325. doi:10.1016/j.cplett.2011.08.079
- [181] D. Music, J. M. Schneider, *New J. Phys.* **2013**, *15*, 073004. doi:10.1088/1367-2630/15/7/073004
- [182] C. Kunze, D. Music, M. T. Baben, J. M. Schneider, G. Grundmeier, *Appl. Surf. Sci.* **2014**, *290*, 504. doi:10.1016/j.apsusc.2013.11.091
- [183] D. Music, D. Lange, L. Raumann, M. T. Baben, F. von Fragstein, J. M. Schneider, *Surf. Sci.* **2012**, *606*, 986. doi:10.1016/j.susc.2012.02.022
- [184] H. Riedl, J. Zálešák, M. Arndt, P. Polcik, D. Holec, P. H. Mayrhofer, *J. Appl. Phys.* **2015**, *118*, 125306. doi:10.1063/1.4931665
- [185] O. A. Shenderova, V. V. Zhirnov, D. W. Brenner, *Crit. Rev. Solid State Mater. Sci.* **2002**, *27*, 227. doi:dx.doi.org/10.1080/10408430208500497
- [186] Y. Huang, J. Wu, K. C. Hwang, *Phys. Rev. B* **2006**, *74*, 245413. doi:10.1103/PhysRevB.74.245413
- [187] M. A. Hartmann, M. Todt, F. G. Rammerstorfer, F. D. Fischer, O. Paris, *Europhys. Lett.* **2013**, *103*, 68004. doi:10.1209/0295-5075/103/68004
- [188] M. Todt, F. G. Rammerstorfer, F. D. Fischer, P. H. Mayrhofer, D. Holec, M. A. Hartmann, *Carbon* **2011**, *49*, 1620. doi:10.1016/j.carbon.2010.12.045
- [189] M. Todt, R. D. Bitsche, M. A. Hartmann, F. D. Fischer, F. G. Rammerstorfer, *Int. J. Solids Struct.* **2014**, *51*, 706. doi:10.1016/j.ijsolstr.2013.10.038
- [190] P. Calaminici, G. Geudtner, A. M. Köster, *J. Chem. Theory Comput.* **2009**, *5*, 29. doi:10.1021/ct800347u
- [191] K. R. Bates, G. E. Scuseria, *Theor. Chem. Acc.* **1998**, *99*, 29.
- [192] D. Holec, P. Dumitraschkewitz, F. D. Fischer, D. Vollath, Size-dependent surface energies of Au nanoparticles arXiv:1412.7195.
- [193] L. Lymperakis, M. Friák, J. Neugebauer, *Eur. Phys. J. Spec. Top.* **2009**, *177*, 41. doi:10.1140/epjst/e2009-01167-6
- [194] M. Všianská, M. Šob, *Phys. Rev. B* **2011**, *84*, 014418. doi:10.1103/PhysRevB.84.014418
- [195] M. Všianská, M. Šob, *Prog. Mater. Sci.* **2011**, *56*, 817. doi:https://doi.org/10.1016/j.pmatsci.2011.01.008
- [196] V. I. Razumovskiy, A. Y. Lozovoi, I. M. Razumovskii, *Acta Mater.* **2015**, *82*, 369. doi:10.1016/j.actamat.2014.08.047
- [197] V. I. Razumovskiy, A. Y. Lozovoi, I. M. Razumovskii, *Acta Mater.* **2016**, *106*, 401. doi:10.1016/j.actamat.2015.12.030
- [198] W. Liu, H. Han, C. Ren, H. Yin, Y. Zou, P. Huai, H. Xu, Effects of rare-earth on the cohesion of Ni Σ 5(012) grain boundary from first-principles calculations, *Comput. Mater. Sci. Part A* **2015**, *96*, 374. doi:10.1016/j.commatsci.2014.09.035
- [199] D. Scheiber, R. Pippin, P. Puschnig, L. Romaner, *Modell. Simul. Mater. Sci. Eng.* **2016**, *24*, 035013. doi:10.1088/0965-0393/24/3/035013

- [200] H. Li, S. Wurster, C. Motz, L. Romaner, C. Ambrosch-Draxl, R. Pippan, *Acta Mater.* **2012**, *60*, 748. doi:10.1016/j.actamat.2011.10.031
- [201] M. Kanani, A. Hartmaier, R. Janisch, *Acta Mater.* **2016**, *106*, 208. doi:10.1016/j.actamat.2015.11.047
- [202] S. Sandlöbes, M. Friák, S. Zaeferrer, A. Dick, S. Yi, D. Letzig, Z. Pei, L.-F. Zhu, J. Neugebauer, D. Raabe, *Acta Mater.* **2012**, *60*, 3011. doi:10.1016/j.actamat.2012.02.006
- [203] S. Sandlöbes, Z. Pei, M. Friák, L.-F. Zhu, F. Wang, S. Zaeferrer, D. Raabe, J. Neugebauer, *Acta Mater.* **2014**, *70*, 92. doi:10.1016/j.actamat.2014.02.011
- [204] Z. Pei, M. Friák, S. Sandlöbes, R. Nazarov, B. Svendsen, D. Raabe, J. Neugebauer, *New J. Phys.* **2015**, *17*, 093009. doi:10.1088/1367-2630/17/9/093009
- [205] Z. Pei, D. Ma, M. Friák, B. Svendsen, D. Raabe, J. Neugebauer, *Phys. Rev. B* **2015**, *92*, 064107. doi:10.1103/PhysRevB.92.064107
- [206] D. Scheiber, R. Pippan, P. Puschnig, A. Ruban, L. Romaner, *Int. J. Refract. Met. Hard Mater.* **2016**, *60*, 75. doi:10.1016/j.ijrmhm.2016.07.003
- [207] X. Wu, X.-S. Kong, Y.-W. You, W. Liu, C. S. Liu, J.-L. Chen, G.-N. Luo, *J. Appl. Phys.* **2016**, *120*, 095901. doi:10.1063/1.4961867
- [208] X. Wu, Y.-W. You, X.-S. Kong, J.-L. Chen, G.-N. Luo, G.-H. Lu, C. S. Liu, Z. Wang, *Acta Mater.* **2016**, *120*, 315. doi:10.1016/j.actamat.2016.08.048
- [209] R. Tran, Z. Xu, N. Zhou, B. Radhakrishnan, J. Luo, S. P. Ong, *Acta Mater.* **2016**, *117*, 91. doi:https://doi.org/10.1016/j.actamat.2016.07.005
- [210] H. Lind, R. Forsén, B. Alling, N. Ghafoor, F. Tasnádi, M. P. Johansson, I. A. Abrikosov, M. Odén, *Appl. Phys. Lett.* **2011**, *99*, 091903. doi:10.1063/1.3631672
- [211] D. Holec, L. Zhou, R. Rachbauer, P. H. Mayrhofer, *J. Appl. Phys.* **2013**, *113*, 113510. doi:10.1063/1.4795590
- [212] W. A. Counts, M. Friák, D. Raabe, J. Neugebauer, *Adv. Eng. Mater.* **2010**, *12*, 1198. doi:10.1002/adem.201000225
- [213] W. A. Counts, M. Friák, D. Raabe, J. Neugebauer, *Adv. Eng. Mater.* **2010**, *12*, 572. doi:10.1002/adem.200900308
- [214] W. Counts, M. Friák, D. Raabe, J. Neugebauer, *Acta Mater.* **2009**, *57*, 69. doi:10.1016/j.actamat.2008.08.03
- [215] D. Raabe, B. Sander, M. Friák, D. Ma, J. Neugebauer, *Acta Mater.* **2007**, *55*, 4475. doi:10.1016/j.actamat.2007.04.024
- [216] W. Setyawan, S. Curtarolo, *Comput. Mater. Sci.* **2010**, *49*, 299. doi:10.1016/j.commatsci.2010.05.010
- [217] H. Lind, F. Tasnádi, I. A. Abrikosov, *New J. Phys.* **2013**, *15*, 095010. doi:10.1088/1367-2630/15/9/095010
- [218] L. J. Nelson, V. Ozoliņš, C. S. Reese, F. Zhou, G. L. W. Hart, *Phys. Rev. B* **2013**, *88*, 155105. doi:10.1103/PhysRevB.88.155105
- [219] D. Howe, M. Costanzo, P. Fey, T. Gojobori, L. Hannick, W. Hide, D. P. Hill, R. Kania, M. Schaeffer, S. St Pierre, S. Twigger, O. White, S. Y. Rhee, *Nature* **2008**, *455*, 47. doi:10.1038/455047a.
- [220] M. de Jong, W. Chen, H. Geerlings, M. Asta, K. A. Persson, *Sci. Data* **2015**, *2*, 150053. doi:10.1038/sdata.2015.53
- [221] M. de Jong, W. Chen, T. Angsten, A. Jain, R. Notestine, A. Gamst, M. Sluiter, C. Krishna Ande, S. van der Zwaag, J. J. Plata, C. Toher, S. Curtarolo, G. Ceder, K. A. Persson, M. Asta, *Sci. Data* **2015**, *2*, 150009. doi:10.1038/sdata.2015.9
- [222] S. Curtarolo, W. Setyawan, S. Wang, J. Xue, K. Yang, R. H. Taylor, L. J. Nelson, G. L. W. Hart, S. Sanvito, M. Buongiorno-Nardelli, N. Mingo, O. Levy, *Comput. Mater. Sci.* **2012**, *58*, 227. doi:10.1016/j.commatsci.2012.02.002
- [223] J. E. Saal, S. Kirklin, M. Aykol, B. Meredig, C. Wolverton, *JOM* **2013**, *65*, 1501. doi:10.1007/s11837-013-0755-4
- [224] G. Pizzi, A. Cepellotti, R. Sabatini, N. Marzari, B. Kozinsky, *Comput. Mater. Sci.* **2016**, *111*, 218. doi:10.1016/j.commatsci.2015.09.013
- [225] A. Jain, S. P. Ong, G. Hautier, W. Chen, W. D. Richards, S. Dacek, S. Cholia, D. Gunter, D. Skinner, G. Ceder, K. A. Persson, *APL Mater.* **2013**, *1*, 011002. doi:10.1063/1.4812323
- [226] S. P. Ong, W. D. Richards, A. Jain, G. Hautier, M. Kocher, S. Cholia, D. Gunter, V. L. Chevrier, K. A. Persson, G. Ceder, *Comput. Mater. Sci.* **2013**, *68*, 314. doi:10.1016/j.commatsci.2012.10.028.
- [227] W. A. Counts, M. Friák, C. C. Battaile, D. Raabe, J. Neugebauer, *Phys. Status Solidi B* **2008**, *245*, 2630. doi:10.1002/pssb.200844226
- [228] M. Friák, T. Hickel, B. Grabowski, L. Lymperakis, A. Udyansky, A. Dick, D. Ma, F. Roters, L. F. Zhu, A. Schlieter, U. Kühn, Z. Ebrahimi, R. A. Lebensohn, D. Holec, J. Eckert, H. Emmerich, D. Raabe, J. Neugebauer, *Eur. Phys. J. Plus* **2011**, *126*, 101. doi:10.1140/epjp/i2011-11101-2
- [229] J. Pavlu, J. Vřešťál, M. Šob, *Modell. Simul. Mater. Sci. Eng.* **2016**, *24*, 025009. doi:10.1088/0965-0393/24/2/025009
- [230] J. Pavlu, J. Vřešťál, M. Šob, *Intermetallics* **2010**, *18*, 212. doi:10.1016/j.intermet.2009.07.018
- [231] D. Ma, M. Friák, J. von Pezold, D. Raabe, J. Neugebauer, *Acta Mater.* **2015**, *85*, 53. doi:10.1016/j.actamat.2014.10.044